Robust a posteriori error control and adaptivity for multiscale, multinumerics, and mortar coupling

Gergina Pencheva, Martin Vohralík, Mary Wheeler, Tim Wildey

ROBUST A POSTERIORI ERROR CONTROL AND ADAPTIVITY FOR MULTISCALE, MULTINUMERICS, AND MORTAR COUPLING*

GERGINA V. PENCHEVA†, MARTIN VOHRALÍK‡, MARY F. WHEELER†, AND TIM WILDEY†

Abstract. We consider discretizations of a model elliptic problem by means of different numerical methods applied separately in different subdomains of the computational domain and coupled using the mortar technique. The subdomain grids need not match along the interfaces. We are also interested in the multiscale setting, where the subdomains are partitioned by a mesh of size h, whereas the interfaces are partitioned by a mesh of much coarser size H, and where lower-order polynomials are used in the subdomains and higher-order polynomials are used on the mortar interface mesh. We derive several fully computable a posteriori error estimates which deliver a guaranteed upper bound on the error measured in the energy norm. Our estimates are also locally efficient and one of them is robust with respect to the ratio H/h under an assumption of sufficient regularity. The present approach allows to bound separately and to compare mutually the subdomain and interface errors. A subdomain/interface adaptive refinement strategy is proposed and numerically tested.

Key words. multiscale, multinumerics, mortar coupling, nonmatching grids, a posteriori error estimate, guaranteed upper bound, robustness, balancing error components

AMS subject classifications. 65N15, 65N30, 76S05

1. Introduction.

We consider in this paper the model problem

$$-\nabla\cdot(\mathbf{K}\nabla p) = f \qquad \text{in } \Omega, \tag{1.1a}$$

$$p = 0 \qquad \text{on } \partial\Omega, \tag{1.1b}$$

where $\Omega \subset \mathbb{R}^d$, $d = 2, 3$, is a polygonal (polyhedral) domain (open, bounded, and connected set), $\mathbf{K}$ is a symmetric, bounded, and uniformly positive definite tensor, and $f \in L^2(\Omega)$. Let Ω be divided into several subdomains. We are interested in discretizations by different numerical methods in the different subdomains. The coupling of these different methods is achieved by the mortar technique. We allow for the cases where the grids of the individual subdomains do not match along the interfaces and where the subdomain grid elements are a mixture of simplices and of rectangular parallelepipeds. We also investigate the case where the size of the subdomain grids, say h, is much smaller than the size of the interface grid, say H. More precisely, we suppose that $H = \mathcal{O}(h^\beta)$ with $\beta < 1$; then lower-order polynomials are used in the subdomain grids and higher-order polynomials are used on the mortar interface mesh. Particular examples of such discretizations are the multiscale mortar mixed finite element method proposed in [6] or the multiscale mortar coupled mixed finite

*A portion of this research was supported by the U.S. Department of Energy, Office of Science, Office of Basic Energy Sciences. The Center for Frontiers of Subsurface Energy Security (CFSES) is a DOE Energy Frontier Research Center, under Contract No. DE-SC0001114. The authors gratefully acknowledge the financial support provided by the NSF-CDI under contract number DMS 0835745 and King Abdullah University of Science and Technology (KAUST)-AEA-UTA08-687 and DOE grant DE-FGO2-04ER25617. The second author was supported by the GNR MoMaS project "Numerical Simulations and Mathematical Modeling of Underground Nuclear Waste Disposal", PACEN/CNRS, ANDRA, BRGM, CEA, EdF, IRSN, France.

†Institute for Computational Engineering and Sciences, University of Texas at Austin, USA (gergina@ices.utexas.edu, mfw@ices.utexas.edu, twildey@ices.utexas.edu).

‡UPMC Univ. Paris 06, UMR 7598, Laboratoire Jacques-Louis Lions, 75005, Paris, France & CNRS, UMR 7598, Laboratoire Jacques-Louis Lions, 75005, Paris, France (vohralik@ann.jussieu.fr).

element–discontinuous Galerkin method of [19]. Note that multiscale mortar techniques are especially appealing as the discretization can be reduced to a problem only involving higher-order polynomials on the interface mortar mesh (see [6]). In addition, this immediately leads to a parallel implementation following [20]. A multiscale mortar basis can be constructed following [18] and multiscale preconditioners can be used following [34]. This leads to their extremely high computational efficiency.

The purpose of this paper is to derive a general framework for optimal a posteriori error estimation in the multiscale, multinumerics, and mortar coupling setting. We derive fully and locally computable estimates providing a guaranteed upper bound on the energy error. We propose several estimators, with increasing complexity of evaluation but with increasing precision. All these estimators are also locally efficient; that is, they also give local lower bounds on the energy error. Importantly, this property holds independently of the use of different discretization schemes in different parts of the domain, of the use of the mortar coupling, and, to a reasonable degree, of the non-alignment of the subdomain meshes at the interfaces. Our estimates are thus robust with respect to the multinumerics and mortar coupling. Moreover, the last of our estimators gives estimates robust with respect to the ratio H/h and is thus robust with respect to the multiscale. We take here up the analysis of [35, 6] while using tools from [30, 33, 17]. For recent results on a posteriori error estimation in multiscale discretizations, we refer to [26, 1, 23] and to the references therein. A posteriori estimates for discretizations with mortar coupling have previously been analyzed in, e.g., [36, 8, 7, 13, 9, 10] and a posteriori estimates for multinumerics in, e.g., [10, 14].

In Section 2, we set up the notation, define the admissible grids, finite-dimensional spaces, and describe the continuous setting. Our a posteriori error estimates are stated in Section 3. We do so in a general setting, not mentioning any particular (combination of) numerical methods employed. We only suppose that we are given an approximate flux $\mathbf{u}_h$ which is $\mathbf{H}(\mathrm{div}, \Omega_i)$-conforming inside each subdomain Ω_i, locally conservative inside each subdomain Ω_i, and whose normal trace is weakly continuous across the interface; see Assumption 3.1. As mentioned earlier, we derive several estimators. Some of them only use the given (nonmatching) grid $\mathcal{T}_h$ and some of them require a construction of a matching grid $\widehat{\mathcal{T}}_h$ and of a globally $\mathbf{H}(\mathrm{div}, \Omega)$-conforming flux $\mathbf{t}_h$. The flux $\mathbf{t}_h$ can be constructed by directly prescribing its degrees of freedom, by solution of low-order-polynomial-degree h-size local Neumann problems, or by solution of high-order-polynomial-degree H-size local Neumann problems by means of the mixed finite element method. All these approaches are described in detail in Section 3.

Section 4 investigates the local efficiency of the derived estimates. Once again, this is done generally, without a specification of the underlying numerical scheme(s); we only need Assumption 4.1 on the weak continuity of the approximate potential $\tilde{p}_h$. Section 5 then gives examples of multiscale, multinumerics, and mortar discretizations. We therein also verify Assumptions 3.1 and 4.1 for each example in question. Sections 6 and 7 respectively collect the proofs of the a posteriori error estimates and of their efficiency. Our estimates allow to distinguish and estimate separately the error coming from the inside of the subdomains and that coming from the mortar coupling; an adaptive algorithm keeping the two error contributions in balance and numerical experiments illustrating the theoretical developments are given in Section 8. (The present estimates can also be used to distinguish and estimate separately the discretization and upscaling errors, cf. Remark 3.9 below.) Appendix A gives a technical result necessary for the analysis on nonmatching grids.

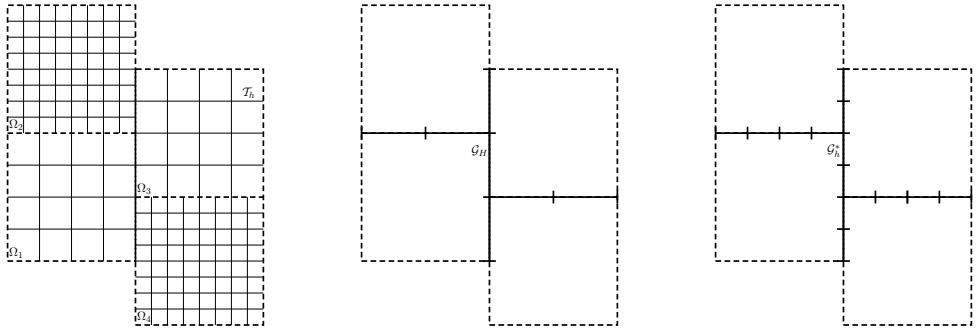

FIG. 2.1. *Example of a domain Ω with subdomains Ω_i and nonmatching mesh $\mathcal{T}_h$ (left), interface mesh $\mathcal{G}_H$ (middle), and the corresponding interface mesh $\mathcal{G}_h^*$ (right)*

2. Preliminaries. We introduce in this section the partitions of Ω, notation, continuous setting, and recall some useful inequalities.

2.1. Partitions of Ω and of Γ. We suppose that Ω is decomposed into nonoverlapping polygonal (polyhedral) subdomains Ω_i, $i \in \{1, \ldots, n\}$. This partition can be nonmatching in the sense that neighboring subdomains need not share complete sides (edges if $d = 2$, faces if $d = 3$). We denote $\Gamma_{i,j} := \partial\Omega_i \cap \partial\Omega_j$, $\Gamma := \cup_{1\le i<j\le n}\Gamma_{i,j}$, and $\Gamma_i := \partial\Omega_i \cap \Gamma$. Let $\mathcal{T}_{h,i}$ be a matching finite element mesh of Ω_i, $i \in \{1, \ldots, n\}$, composed of simplices and rectangular parallelepipeds. A mixture of triangles and rectangles is allowed for $d = 2$ but we only allow for either tetrahedra or rectangular parallelepipeds for $d = 3$ (we would need to introduce other elements like prisms for $d = 3$ in order to allow for mixture grids, which we prefer to avoid for the sake of simplicity). We then set $\mathcal{T}_h := \cup_{i=1}^n \mathcal{T}_{h,i}$ and denote by h the maximal element diameter in $\mathcal{T}_h$; note that $\mathcal{T}_h$ can be nonmatching as neighboring meshes $\mathcal{T}_{h,i}$ and $\mathcal{T}_{h,j}$ need not align on $\Gamma_{i,j}$. A generic element of the partition $\mathcal{T}_h$ will be denoted by T; h_T stands for the diameter of T. This setting is illustrated in Figure 2.1 (left).

We use $\mathcal{E}_{h,i}^{\rm int}$ to denote the interior sides of $\mathcal{T}_{h,i}$, $i \in \{1, \ldots, n\}$, and set $\mathcal{E}_h^{\rm int} := \cup_{i=1}^n \mathcal{E}_{h,i}^{\rm int}$; $\mathcal{E}_h^{\rm int}$ thus contains neither the subdomain interfaces nor the outer boundary of Ω. We denote by $\mathcal{E}_{h,i}$ all the sides of $\mathcal{T}_{h,i}$ and set $\mathcal{E}_h := \cup_{i=1}^n \mathcal{E}_{h,i}$. We let $\mathcal{E}_{h,i,j}^{\Gamma}$ be the partition of $\Gamma_{i,j}$ by the sides of $\mathcal{T}_{h,i}$ and $\mathcal{E}_{h,i}^{\Gamma}$ the partition of Γ_i by the sides of $\mathcal{T}_{h,i}$. We denote by $\mathcal{E}_h^{\Gamma} := \cup_{1\le i\le n}\mathcal{E}_{h,i}^{\Gamma}$ all the sides of $\mathcal{T}_h$ located at the interface Γ and by $\mathcal{E}_h^{\rm ext} := \mathcal{E}_h \setminus \mathcal{E}_h^{\rm int} \setminus \mathcal{E}_h^{\Gamma}$ the faces of $\mathcal{T}_h$ located at the boundary of Ω. We also set $\mathcal{E}_h^{{\rm int},\Gamma} := \mathcal{E}_h^{\rm int} \cup \mathcal{E}_h^{\Gamma}$. The notation $\mathcal{E}_T$ stands for all the sides of en element $T \in \mathcal{T}_h$. A generic side of $\mathcal{E}_h$ will be denoted by e and its diameter by h_e.

Next, we let $\mathcal{G}_{H,i,j}$ be the mortar interface finite element mesh of $\Gamma_{i,j}$. The elements $g \in \mathcal{G}_{H,i,j}$ are either line segments (if $d = 2$) or triangles or rectangles (if $d = 3$). We do not require $\mathcal{G}_{H,i,j}$ to be matching in the sense of a $(d-1)$-dimensional mesh of $\Gamma_{i,j}$. We set $\mathcal{G}_{H,i} := \cup_{1\le j\le n}\mathcal{G}_{H,i,j}$ and $\mathcal{G}_H := \cup_{1\le i<j\le n}\mathcal{G}_{H,i,j}$, cf. Figure 2.1 (middle). Maximal element diameter in $\mathcal{G}_H$ is denoted by H. In the multiscale setting, $h < H \le 1$ and the ratio H/h can be unbounded, $H = \mathcal{O}(h^\beta)$ with $\beta < 1$. Note that on an interface $\Gamma_{i,j}$, $\mathcal{G}_{H,i,j}$ is a unique $(d-1)$-dimensional surface mesh, whereas there are two (different) meshes $\mathcal{E}_{h,i,j}^{\Gamma}$ and $\mathcal{E}_{h,j,i}^{\Gamma}$ from the two sides of the interface. Also, the meshes $\mathcal{E}_{h,i,j}^{\Gamma}$ and $\mathcal{E}_{h,j,i}^{\Gamma}$ need in general not be refinements of $\mathcal{G}_{H,i,j}$; we will, however, need such a requirement at some occasions later. We also assume that the intersection of the meshes $\mathcal{E}_{h,i,j}^{\Gamma}$ and $\mathcal{E}_{h,j,i}^{\Gamma}$ is a matching mesh of $\Gamma_{i,j}$ consisting of line segments (if $d = 2$) or triangles or rectangles (if $d = 3$), such that for any of its

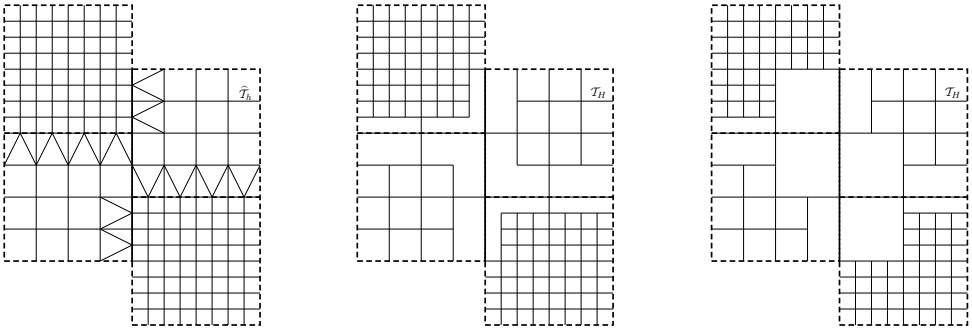

FIG. 2.2. *Example of a matching refinement $\widehat{\mathcal{T}}_h$ of $\mathcal{T}_h$ (left), of a nonmatching and not shape-regular mesh $\mathcal{T}_H$ (middle), and of its modification avoiding nonconvex elements (right)*

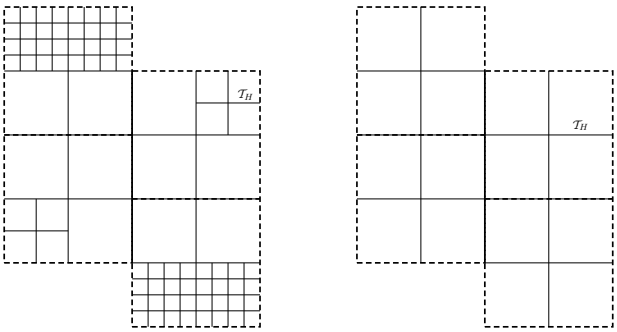

FIG. 2.3. *Example of a shape-regular but nonmatching mesh $\mathcal{T}_H$ (left) and of a matching and shape-regular mesh $\mathcal{T}_H$ (right)*

element T, the ratio $|T|/|T'|$ for any element T' of $\mathcal{E}_{h,i,j}^{\Gamma}$ or $\mathcal{E}_{h,j,i}^{\Gamma}$ is bounded.

We will in the sequel also use the following partition of Γ. Let an interface $\Gamma_{i,j}$ be given. We define the mesh $\mathcal{G}_{h,i,j}^{*}$ as a set of $(d-1)$-dimensional sides g, where each $g \in \mathcal{G}_{h,i,j}^{*}$ is simultaneously a union of sides from $\mathcal{E}_{h,i,j}^{\Gamma}$ and a union of sides from $\mathcal{E}_{h,j,i}^{\Gamma}$. We choose the sides g so as to be composed of a smallest possible number of sides from $\mathcal{E}_{h,i,j}^{\Gamma}$ and $\mathcal{E}_{h,j,i}^{\Gamma}$. There is one mesh $\mathcal{G}_{h,i,j}^{*}$ for each interface $\Gamma_{i,j}$. We set $\mathcal{G}_{h,i}^{*} := \cup_{1\le j\le n}\mathcal{G}_{h,i,j}^{*}$ and $\mathcal{G}_{h}^{*} := \cup_{1\le i<j\le n}\mathcal{G}_{h,i,j}^{*}$, cf. Figure 2.1 (right). We denote by H_g the diameter of a side $g \in \mathcal{G}_H$ and by h_g the diameter of a side $g \in \mathcal{G}_h^{*}$. We suppose that there exists a positive constant $C_{\mathcal{G}_h^{*}}$ such that, for all $g \in \mathcal{G}_h^{*}$,

$$\frac{h_g}{h_e} \le C_{\mathcal{G}_h^{*}} \qquad \forall e \in \mathcal{E}_h^{\Gamma},\, e \subset g. \tag{2.1}$$

Assuming (2.1), we avoid the case where h_g/h_e is only bounded by a function of H/h.

Finally, two other types of partitions of Ω will be used in the paper. Firstly, $\widehat{\mathcal{T}}_h$ is a matching refinement of $\mathcal{T}_h$, consisting of simplices and rectangular parallelepipeds (as for $\mathcal{T}_h$, mixture grids are allowed for $d = 2$). We refer to Figure 2.2 (left) for an example of $\widehat{\mathcal{T}}_h$. We denote by $\widehat{\mathcal{E}}_h$ the sides of $\widehat{\mathcal{T}}_h$ and use the notation $\widehat{\mathcal{T}}_{h,i}$ for the restriction of $\widehat{\mathcal{T}}_h$ on the subdomain Ω_i. We suppose that $\widehat{\mathcal{T}}_{h,i}$ coincides with $\mathcal{T}_{h,i}$ in the interior of each subdomain Ω_i and only differs from $\widehat{\mathcal{T}}_h$ near the interfaces. More precisely, we assume that for each $T \in \mathcal{T}_h$ such that $T \cap \Gamma = \emptyset$, there exists an element

$T' \in \widehat{\mathcal{T}}_h$ such that $T = T'$. We also assume that every side $e' \in \widehat{\mathcal{E}}_h$ which shares a node with this T' either coincides with some side $e \in \mathcal{E}_h^{\rm int}$ or belongs to the interior of some $T'' \in \mathcal{T}_h$. Finally, we assume that $\widehat{\mathcal{T}}_h$ adds no new nodes and sides at the interface Γ in comparison with $\mathcal{T}_h$. The last mesh used is denoted by $\mathcal{T}_H$. It will be in general formed by groups of elements from $\mathcal{T}_h$ and it will differ in different approaches. It may be matching or nonmatching, shape-regular (cf. Section 4 for our definition of shape-regularity) or not; it's characteristic feature is that the restriction of $\mathcal{T}_H$ on Γ is the interface mesh $\mathcal{G}_H$. As before, we use the notation $\mathcal{T}_{H,i}$ for the restriction of $\mathcal{T}_H$ on Ω_i. We refer to Figure 2.2 (middle and right) and to Figure 2.3 for examples of different meshes $\mathcal{T}_H$. For an element $T \in \mathcal{T}_H$, we denote by $\mathcal{G}_T$ the set of its sides.

2.2. Finite-dimensional spaces and projection operators. We begin with the mortar space M_H. It is the space of discontinuous piecewise polynomials of order m on the interface mesh $\mathcal{G}_H$; M_H thus in particular contains piecewise constant functions on $\mathcal{G}_H$. We next define the spaces on $\mathcal{T}_h$. If $T \in \mathcal{T}_h$ is a simplex, we let $\mathbb{R}_r(T) := \mathbb{P}_r(T)$ be the space of polynomials of total degree at most r. If $T \in \mathcal{T}_h$ is a rectangular parallelepiped, we let $\mathbb{R}_r(T) := \mathbb{Q}_r(T)$ be the space of polynomials of degree at most r in each variable. We then define $\mathbb{R}_r(\mathcal{T}_h)$ as the space such that for each $w \in \mathbb{R}_r(\mathcal{T}_h)$, $w|_T \in \mathbb{R}_r(T)$; we require no continuity at the sides. We also define $\mathbb{R}_{k-1,*,d}(T)$ by $[\mathbb{P}_{k-1}(T)]^d$ for a simplex and $\mathbb{Q}_{k-1,k}(T) \times \mathbb{Q}_{k,k-1}(T)$ if $d = 2$ and $\mathbb{Q}_{k-1,k,k}(T) \times \mathbb{Q}_{k,k-1,k}(T) \times \mathbb{Q}_{k,k,k-1}(T)$ if $d = 3$ for a rectangular parallelepiped. Let $\mathbf{V}_{h,i} \times W_{h,i} \subset \mathbf{H}(\mathrm{div}, \Omega_i) \times L^2(\Omega_i)$ be the Raviart–Thomas–Nédélec (RTN) mixed finite element spaces of order k, $\mathbf{V}_{h,i} := \mathbf{RTN}^k(\mathcal{T}_{h,i})$, $W_{h,i} := \mathbb{R}_k(\mathcal{T}_{h,i})$, cf. [11, 28]. The present theory can easily be extended to other mixed finite element spaces. We can also easily take into account spaces with different polynomial degrees in different subdomains and also with different polynomial degrees in different elements; we restrict ourselves to the given setting for the sakes of brevity and clarity. We then set $\mathbf{V}_h := \bigoplus_{i=1}^n \mathbf{V}_{h,i}$, $W_h := \bigoplus_{i=1}^n W_{h,i}$. Note that the normal components of vectors in $\mathbf{V}_h$ are continuous across the sides between elements in each subdomain Ω_i but not across Γ. Based on these spaces, we will also use $\mathbf{V}_{\widehat{h}}$, the RTN space on the matching submesh $\widehat{\mathcal{T}}_h$ of $\mathcal{T}_h$, and $W_{\widehat{h}}$, the W_h equivalent on $\widehat{\mathcal{T}}_h$. We keep the same order k when both $\mathcal{T}_h$ and $\widehat{\mathcal{T}}_h$ are simplicial. When $\widehat{\mathcal{T}}_h$ contains simplices cutting rectangular parallelepipeds (as in Figure 2.2 (left)) and when using the approach of Section 3.3.2 below, we have to appropriately increase the space order to k' in $\mathbf{V}_{\widehat{h}}$ and $W_{\widehat{h}}$, see (3.20a). In the case where $\mathcal{T}_H$ is matching and shape-regular, $\mathbf{V}_H$ stands for the m-th order RTN space on the coarse mesh $\mathcal{T}_H$ and W_H for the W_h equivalent on $\mathcal{T}_H$. We use the notation $V(S)$ for the restriction of some space V, a priori defined on the whole Ω/mesh $\mathcal{T}_h$, to the subdomain/submesh S.

We will also need some orthogonal projections: let P_{W_h} be the $L^2(\Omega)$-orthogonal projection onto W_h, $P_{W_{\widehat{h}}}$ the $L^2(\Omega)$-orthogonal projection onto $W_{\widehat{h}}$, P_{W_H} the $L^2(\Omega)$-orthogonal projection onto W_H, and P_{M_H} the $L^2(\Gamma)$-orthogonal projection onto M_H,

$$
\begin{aligned}
&P_{W_h} : L^2(\Omega) \to W_h && \text{for } w \in L^2(\Omega), && (w - P_{W_h}(w), w_h) = 0 && \forall w_h \in W_h,\\
&P_{W_{\widehat{h}}} : L^2(\Omega) \to W_{\widehat{h}} && \text{for } w \in L^2(\Omega), && (w - P_{W_{\widehat{h}}}(w), w_h) = 0 && \forall w_h \in W_{\widehat{h}},\\
&P_{W_H} : L^2(\Omega) \to W_H && \text{for } w \in L^2(\Omega), && (w - P_{W_H}(w), w_H) = 0 && \forall w_H \in W_H,\\
&P_{M_H} : L^2(\Gamma) \to M_H && \text{for } \mu \in L^2(\Gamma), && (\mu - P_{M_H}(\mu), \mu_H)_\Gamma = 0 && \forall \mu_H \in M_H.
\end{aligned}
$$

We also denote by π_l the orthogonal projection onto $\mathbb{R}_l(\mathcal{T})$ ($\mathcal{T}$ is the mesh in question).

2.3. Other notation. Let $D \subset \Omega$. Then $\|\cdot\|_D$ stands for the $L^2(D)$ norm and $(\cdot,\cdot)_D$ for the $L^2(D)$ scalar product. Shall D coincide with Ω, the subscript D will be dropped. The $L^2(D)$ scalar product for $D \subset \mathbb{R}^{d-1}$ will be denoted by $\langle\cdot,\cdot\rangle_D$. We also use the notation $|D|$ for the $(d-1)$-dimensional Lebesgue measure of $D \subset \mathbb{R}^{d'}$, $1 \le d' \le d$. For $v \in L^1(D)$, we denote by v_D the mean value of v on D. For $D \subset \Omega$, we denote by $c_{\mathbf{K},D}$, $C_{\mathbf{K},D}$ the smallest and largest eigenvalue of $\mathbf{K}$ on D, respectively.

For a sufficiently smooth function v that is double-valued on an interior side $e \in \mathcal{E}_h^{\mathrm{int}}$, $e = T^- \cap T^+$, its jump and average on e are defined as

$$[\![v]\!] := v|_{T^-} - v|_{T^+}, \qquad \{\!\{v\}\!\} := \tfrac{1}{2}(v|_{T^-} + v|_{T^+}). \tag{2.3}$$

We set $[\![v]\!] := v|_e$ and $\{\!\{v\}\!\} := v|_e$ for $e \in \mathcal{E}_h^{\mathrm{ext}}$. We use similar notation for the sides g from $\mathcal{G}_H$ and $\mathcal{G}_h^*$ and also for the sides e from $\widehat{\mathcal{E}}_h$. For each side $e \in \mathcal{E}_h^{\mathrm{int}}$, $g \in \mathcal{G}_H$, or $g \in \mathcal{G}_h^*$, we use the notation $\mathbf{n}_e$, $\mathbf{n}_g$ for the unit normal vector, pointing from T^- towards T^+. Similarly, $\mathbf{n}_\Gamma$ stands for the unit normal vector to Γ, with arbitrary but fixed orientation. For boundary sides e, $\mathbf{n}_e$ coincides with the unit normal vector, outward to Ω. Similarly, for $D \subset \Omega$, $\mathbf{n}_D$ is systematically used to denote the unit normal vector, outward to D.

2.4. Bilinear form, weak solution, energy norm. Let the symmetric bilinear form $\mathcal{A}$ be given by

$$\mathcal{A}(\mathbf{u},\mathbf{v}) := (\mathbf{u}, \mathbf{K}^{-1}\mathbf{v}), \qquad \mathbf{u},\mathbf{v} \in \mathbf{L}^2(\Omega). \tag{2.4}$$

The weak solution of (1.1a)–(1.1b) is $p \in H_0^1(\Omega)$ such that

$$\mathcal{A}(\mathbf{K}\nabla p, \mathbf{K}\nabla\varphi) = (f,\varphi) \qquad \forall \varphi \in H_0^1(\Omega). \tag{2.5}$$

Recall that $\mathbf{u} := -\mathbf{K}\nabla p$ is the weak flux satisfying $\mathbf{u} \in \mathbf{H}(\mathrm{div},\Omega)$. Let $H^1(\mathcal{T}_h) := \{\varphi \in L^2(\Omega);\, \varphi|_T \in H^1(T)\ \forall T \in \mathcal{T}_h\}$ be the broken Sobolev space. We will use the sign ∇ to denote the elementwise gradient. We define the energy seminorm on $H^1(\mathcal{T}_h)$

$$|||\varphi|||^2 := \mathcal{A}(\mathbf{K}\nabla\varphi, \mathbf{K}\nabla\varphi) = \left\|\mathbf{K}^{\frac{1}{2}}\nabla\varphi\right\|^2, \qquad \varphi \in H^1(\mathcal{T}_h), \tag{2.6}$$

and the energy norm on $\mathbf{L}^2(\Omega)$ by

$$|||\mathbf{v}|||_*^2 := \mathcal{A}(\mathbf{v},\mathbf{v}) = \left\|\mathbf{K}^{-\frac{1}{2}}\mathbf{v}\right\|^2, \qquad \mathbf{v} \in \mathbf{L}^2(\Omega). \tag{2.7}$$

2.5. Poincaré and trace inequalities. We recall here two basic inequalities necessary in order to obtain our a posteriori error estimates. Let T be an element of any of the finite element partitions considered, e its side, and $\varphi \in H^1(T)$. Firstly, Poincaré's inequality states that

$$\|\varphi - \varphi_T\|_T \le C_{\mathrm{P},T} h_T \|\nabla\varphi\|_T. \tag{2.8}$$

The constant $C_{\mathrm{P},T}$ is equal to $1/\pi$ whenever T is convex. Secondly, the trace inequality states that

$$\|\varphi - \varphi_e\|_e \le C_{\mathrm{t},T,e} h_e^{\frac{1}{2}} \|\nabla\varphi\|_T. \tag{2.9}$$

It has been shown in [25, Lemma 3.5] that $C_{\mathrm{t},T,e} = (C_{\mathrm{t},d})^{\frac{1}{2}}(|e|h_T^2/(|T|h_e))^{\frac{1}{2}}$, where $C_{\mathrm{t},d} \approx 0.77708$ for a triangle, $C_{\mathrm{t},d} \approx 3.84519$ for a tetrahedron, and $C_{\mathrm{t},d} = 1/(\pi\tanh\pi)$ for a rectangle.

3. A posteriori error estimates. We present in this section a general framework for a posteriori error estimates in the multiscale, multinumerics, and mortar coupling setting. We propose several guaranteed and fully computable estimates and we discuss their practical evaluation.

We present the results in a general setting, not relying on any particular discretization method. Recall that the meshes $\mathcal{T}_h$ and $\mathcal{G}_H$ and the space $\mathbf{V}_h$ are introduced in Section 2. We only make the following assumption:

ASSUMPTION 3.1 (Properties of $\mathbf{u}_h$). *Let*

1. $\mathbf{u}_h \in \mathbf{V}_h$;
2. $(\nabla\cdot\mathbf{u}_h, 1)_T = (f,1)_T \qquad \forall T \in \mathcal{T}_h$;
3. $\sum_{i=1}^{n} \langle \mathbf{u}_h\cdot\mathbf{n}_{\Omega_i}, \mu_H\rangle_{\Gamma_i} = 0 \qquad \forall \mu_H \in M_H$.

Assumption 3.1 means that the approximate flux $\mathbf{u}_h$ is $\mathbf{H}(\mathrm{div},\Omega_i)$-conforming inside each subdomain Ω_i, locally conservative inside each subdomain Ω_i on the elements of $\mathcal{T}_{h,i}$, and that its normal trace is weakly continuous across the interface sides. We will, in fact, still weaken this assumption in some of the results below.

3.1. Estimates for the flux. We first state estimates for the error in the flux $\mathbf{u}_h$. We need to introduce some more notation. Let $\mathcal{T}_H$ be a coarse-scale mesh as introduced in Section 2.1. This mesh is only needed in order to state the following estimate, it is not needed for the computation of $\mathbf{u}_h$. For a given subdomain Ω_i and a given interface side $g \in \mathcal{G}_{H,i}$, let $T_{i,g}$ denote the element of $\mathcal{T}_{H,i}$ having g as a side. We assume that the elements $T_{i,g}$, $g \in \mathcal{G}_{H,i}$, $i \in \{1,\ldots,n\}$, do not overlap. Such a mesh $\mathcal{T}_H$ can always be constructed; remark also that the choice of $\mathcal{T}_H$ is not unique. For a given $i \in \{1,\ldots,n\}$, $g \in \mathcal{G}_{H,i}$, and the associated $T_{i,g} \in \mathcal{T}_{H,i}$, recall that we have the trace inequality (2.9) with the constant $C_{\mathrm{t},T_{i,g},g}$. For a given $T \in \mathcal{T}_h$, recall that we have Poincaré's inequality (2.8) with the constant $C_{\mathrm{P},T}$. The first result is:

THEOREM 3.2 (A "mortar" estimate for the flux). *Let* $\mathbf{u}$ *be the exact flux and let* $\mathbf{u}_h$ *satisfy Assumption 3.1. Pick an arbitrary* $s_h \in H^1_0(\Omega)$. *Then*

$$|||\mathbf{u}-\mathbf{u}_h|||_* \le \eta_{\mathrm{P}} + \eta_{\mathrm{R},h} + \eta_{\mathrm{M}},$$

where the potential, residual, *and* mortar estimators *are given respectively by*

$$\eta_{\mathrm{P}} := |||\mathbf{u}_h + \mathbf{K}\nabla s_h|||_*, \tag{3.1}$$

$$\eta_{\mathrm{R},h} := \left\{ \sum_{T\in\mathcal{T}_h} C^2_{\mathrm{P},T} h_T^2 c^{-1}_{\mathbf{K},T} \|f - \nabla\cdot\mathbf{u}_h\|^2_T \right\}^{\frac12}, \tag{3.2}$$

$$\eta_{\mathrm{M}} := \left\{ \sum_{i=1}^{n}\sum_{j=1}^{n} \sum_{g\in\mathcal{G}_{H,i,j}} \left(\tfrac12 \|[\![\mathbf{u}_h\cdot\mathbf{n}_g]\!]\|_g C_{\mathrm{t},T_{i,g},g} H_g^{\frac12} c^{-\frac12}_{\mathbf{K},T_{i,g}} \right)^2 \right\}^{\frac12}. \tag{3.3}$$

Theorem 3.2 gives a guaranteed upper bound on the error $|||\mathbf{u}-\mathbf{u}_h|||_*$. It contains the mortar estimate η_{M} which clearly corresponds to the discontinuity of the normal component of $\mathbf{u}_h$ across the subdomain interfaces. It is thus possible to distinguish the error component stemming from the subdomain discretization error (η_{P} and $\eta_{\mathrm{R},h}$) and the one due to the mortar coupling at the subdomain interfaces (η_{M}) and to adaptively decide whether the subdomain or mortar approximation should be improved. The estimate of Theorem 3.2 may, however, overestimate the mortar error since it is based on the trace inequality (2.9) and features the (known) constant $C_{\mathrm{t},T_{i,g},g}$.

In order to possibly improve on this point, we also present the following theorem (here $\mathcal{T}_H$ is either a coarse-scale or a fine-scale partition of Ω, to be determined later):

THEOREM 3.3 (An optimal estimate for the flux). *Let* $\mathbf{u}$ *be the exact flux and let* $\mathbf{u}_h \in \mathbf{L}^2(\Omega)$ *be arbitrary. Pick an arbitrary* $s_h \in H_0^1(\Omega)$ *and let* $\mathbf{t}_h \in \mathbf{H}(\mathrm{div},\Omega)$ *be arbitrary but such that*

$$(\nabla\cdot\mathbf{t}_h, 1)_T = (f,1)_T \qquad \forall T \in \mathcal{T}_H. \tag{3.4}$$

Then

$$|||\mathbf{u}-\mathbf{u}_h|||_* \le \eta_{\mathrm{P}} + \eta_{\mathrm{R},H} + \tilde{\eta}_{\mathrm{M}}, \tag{3.5}$$

where η_{P} *is given by* (3.1) *and*

$$\eta_{\mathrm{R},H} := \left\{ \sum_{T\in\mathcal{T}_H} C_{\mathrm{P},T}^2 H_T^2 c_{\mathbf{K},T}^{-1} \|f-\nabla\cdot\mathbf{t}_h\|_T^2 \right\}^{\frac{1}{2}}, \tag{3.6}$$

$$\tilde{\eta}_{\mathrm{M}} := |||\mathbf{u}_h - \mathbf{t}_h|||_*. \tag{3.7}$$

We remark that the nature of the above estimate is clear. Instead of η_{P} and $\tilde{\eta}_{\mathrm{M}}$, respectively, it can be written with $\inf_{s_h\in H_0^1(\Omega)} |||\mathbf{u}_h+\mathbf{K}\nabla s_h|||_*$ and $\inf_{\mathbf{t}_h} |||\mathbf{u}_h-\mathbf{t}_h|||_*$, where $\mathbf{t}_h$ are to be taken in $\mathbf{H}(\mathrm{div},\Omega)$ and such that $(\nabla\cdot\mathbf{t}_h,1)_T = (f,1)_T$ for all $T\in\mathcal{T}_H$. Then the first term corresponds to the fact that $\mathbf{u}_h \ne -\mathbf{K}\nabla s_h$ for some $s_h \in H_0^1(\Omega)$, which is which is the case for the exact flux, whereas the second term corresponds to the facts that $\mathbf{u}_h \notin \mathbf{H}(\mathrm{div},\Omega)$ and $\nabla\cdot\mathbf{u}_h \ne f$.

3.2. Estimates for the potential. We state here our estimates for the error in the potential. We present them for a general potential approximation $\tilde{p}_h \in H^1(\mathcal{T}_h)$.

THEOREM 3.4 (A "mortar" estimate for the potential). *Let* p *be the exact potential, let* $\tilde{p}_h \in H^1(\mathcal{T}_h)$ *be arbitrary, and let* $\mathbf{u}_h$ *satisfy Assumption 3.1. Pick an arbitrary* $s_h \in H_0^1(\Omega)$. *Then*

$$|||p-\tilde{p}_h||| \le \eta_{\mathrm{NC}} + \eta_{\mathrm{R},h} + \eta_{\mathrm{M}} + \eta_{\mathrm{DF}},$$

where $\eta_{\mathrm{R},h}$ *is given by* (3.2), η_{M} *by* (3.3), *and the* nonconformity *and* diffusive flux estimators *are given respectively by*

$$\eta_{\mathrm{NC}} := |||\tilde{p}_h - s_h|||, \tag{3.8}$$

$$\eta_{\mathrm{DF}} := |||\mathbf{K}\nabla\tilde{p}_h + \mathbf{u}_h|||_*. \tag{3.9}$$

As in Section 3.1, the following improved version of Theorem 3.4 holds (here $\mathcal{T}_H$ is as in Theorem 3.3):

THEOREM 3.5 (An optimal estimate for the potential). *Let* p *be the exact potential and let* $\tilde{p}_h \in H^1(\mathcal{T}_h)$ *be arbitrary. Pick an arbitrary* $s_h \in H_0^1(\Omega)$ *and let* $\mathbf{t}_h \in \mathbf{H}(\mathrm{div},\Omega)$ *be arbitrary but such that* (3.4) *holds. Then*

$$|||p-\tilde{p}_h||| \le \eta_{\mathrm{NC}} + \eta_{\mathrm{R},H} + \eta_{\mathrm{DFM}}, \tag{3.10}$$

with η_{NC} *given by* (3.8), $\eta_{\mathrm{R},H}$ *by* (3.6), *and the* diffusive flux–mortar estimator *by*

$$\eta_{\mathrm{DFM}} := |||\mathbf{K}\nabla\tilde{p}_h + \mathbf{t}_h|||_*. \tag{3.11}$$

The nature of the estimate is again clear: we can replace $\eta_{\rm NC}$ by $\inf_{s_h\in H^1_0(\Omega)}|||\tilde p_h - s_h|||$ which corresponds to the fact that $\tilde p_h \notin H^1_0(\Omega)$, which is the case for the exact potential. Similarly, one can write the estimate with $\inf_{\mathbf{t}_h}|||\mathbf{K}\nabla\tilde p_h + \mathbf{t}_h|||_*$ with $\mathbf{t}_h \in \mathbf{H}(\mathrm{div},\Omega)$ and $(\nabla\cdot\mathbf{t}_h,1)_T = (f,1)_T$ for all $T\in\mathcal{T}_H$, which corresponds to the facts that $\mathbf{K}\nabla\tilde p_h \notin \mathbf{H}(\mathrm{div},\Omega)$ and $-\nabla\cdot(\mathbf{K}\nabla\tilde p_h)\neq f$, which is the case for the exact potential. Note that, by the triangle inequality, $\eta_{\rm DFM}\le\eta_{\rm DF}+\tilde\eta_{\rm M}$, so that we can once again distinguish the subdomain and interface errors.

REMARK 3.6 (Residual estimator $\eta_{{\rm R},H}$). *Recall $P_{W_{\widehat{\mathcal{T}}_h}}$ and P_{W_H} of Section 2.2. We will meet particular cases where $\mathbf{t}_h$ of Theorems 3.3 and 3.5 will be such that*

$$\nabla\cdot\mathbf{t}_h = P_{W_{\widehat{\mathcal{T}}_h}}(f). \tag{3.12}$$

Then we can set $\mathcal{T}_H := \widehat{\mathcal{T}}_h$ in Theorems 3.3 and 3.5 and replace $\eta_{{\rm R},H}$ of (3.6) by

$$\eta_{{\rm R},\widehat{\mathcal{T}}_h} := \left\{\sum_{T\in\widehat{\mathcal{T}}_h} C_{{\rm P},T}^2 h_T^2 c_{\mathbf{K},T}^{-1}\|f - P_{W_{\widehat{\mathcal{T}}_h}}(f)\|_T^2\right\}^{\frac12}. \tag{3.13}$$

Note that $\eta_{{\rm R},\widehat{\mathcal{T}}_h}$ takes the form of the usual data oscillation estimate on the mesh $\widehat{\mathcal{T}}_h$.

We will also meet cases where $\mathbf{t}_h$ of Theorems 3.3 and 3.5 will be such that

$$\nabla\cdot\mathbf{t}_h = P_{W_H}(f). \tag{3.14}$$

Then the residual estimator $\eta_{{\rm R},H}$ of (3.6) takes the form

$$\eta_{{\rm R},H} = \left\{\sum_{T\in\mathcal{T}_H} C_{{\rm P},T}^2 H_T^2 c_{\mathbf{K},T}^{-1}\|f - P_{W_H}(f)\|_T^2\right\}^{\frac12}. \tag{3.15}$$

Note that such $\eta_{{\rm R},H}$ takes the form of the data oscillation on the mesh $\mathcal{T}_H$.

REMARK 3.7 (Theorems 3.2–3.5). *In Theorems 3.2 and 3.4, only the meshes $\mathcal{T}_h$ and $\mathcal{G}_H$ are needed (the mesh $\widehat{\mathcal{T}}_h$ introduced in Section 2.1 may be employed for the construction of the the potential reconstruction s_h when $\mathcal{T}_h$ is nonmatching). For Theorems 3.3 and 3.5, the meshes $\widehat{\mathcal{T}}_h$ (when $\mathcal{T}_h$ is nonmatching) and $\mathcal{T}_H$ introduced in Section 2.1 and specified in Section 3.3 below are essential. Note also that the potential reconstruction s_h is needed in all Theorems 3.2–3.5, whereas the flux reconstruction $\mathbf{t}_h$ is only needed in Theorems 3.3 and 3.5.*

REMARK 3.8 (Necessity to practically construct s_h and $\mathbf{t}_h$). *The a posteriori error estimators above only involve norms featuring the reconstructions s_h and $\mathbf{t}_h$. Following, e.g., [4], there may be ways how to compute these estimators (evaluate these norms) without the need to practically construct s_h and $\mathbf{t}_h$.*

REMARK 3.9 (Upscaling of $\mathbf{K}$ and the associated error). *In the present setting, $\mathbf{K}$ is not related to the fine-scale mesh $\mathcal{T}_h$ nor to any coarse-scale mesh $\mathcal{T}_H$ (it is not supposed to be, for example, piecewise constant or piecewise polynomial on some mesh). In practice, some upscaled version $\mathbf{K}_{\rm upsc}$ of $\mathbf{K}$ (for instance, piecewise polynomial on $\mathcal{T}_H$) may be used to obtain $\mathbf{u}_h$ (and $\tilde p_h$). We then can estimate*

$$\begin{aligned}\eta_{\rm P} =& \|\mathbf{K}^{-\frac12}(\mathbf{u}_h+\mathbf{K}\nabla s_h)\| \le \|(\mathbf{K}^{-\frac12}-\mathbf{K}_{\rm upsc}^{-\frac12})\mathbf{u}_h\| + \|(\mathbf{K}^{\frac12}-\mathbf{K}_{\rm upsc}^{\frac12})\nabla s_h\|\\ &+\|\mathbf{K}_{\rm upsc}^{-\frac12}(\mathbf{u}_h+\mathbf{K}_{\rm upsc}\nabla s_h)\|,\end{aligned}$$

where the first two terms represent the upscaling error *and the last term the* discretization error. *Similar estimates can be devised for the other estimators.*

We will consider below the restrictions of the different estimators to each element T, denoted by $\eta_{\cdot,T}$. Similarly, for $g \in \mathcal{G}_{H,i,j}$, we set

$$\eta_{\mathrm{M},g} := \|[\![\mathbf{u}_h \cdot \mathbf{n}_g]\!]\|_g H_g^{\frac{1}{2}} \left\{ \left(\tfrac{1}{2} C_{\mathrm{t},T_{i,g},g} c_{\mathbf{K},T_{i,g}}^{-\frac{1}{2}} \right)^2 + \left(\tfrac{1}{2} C_{\mathrm{t},T_{j,g},g} c_{\mathbf{K},T_{j,g}}^{-\frac{1}{2}} \right)^2 \right\}^{\frac{1}{2}}. \tag{3.16}$$

3.3. Practical construction of $H_0^1(\Omega)$- and $\mathbf{H}(\mathrm{div},\Omega)$-conforming reconstructions. We describe here practical constructions of $H_0^1(\Omega)$-conforming reconstruction s_h figuring in Theorems 3.2–3.5 and of $\mathbf{H}(\mathrm{div},\Omega)$-conforming reconstruction $\mathbf{t}_h$ figuring in Theorems 3.3 and 3.5. We only propose one way of constructing s_h but we derive several ways of constructing $\mathbf{t}_h$.

Let $g \in \mathcal{G}_{H,i,j}$. Then Assumption 3.1 (3) implies

$$\langle [\![\mathbf{u}_h \cdot \mathbf{n}_g]\!], \mu_g \rangle_g = 0 \qquad \forall \mu_g \in M_H(g). \tag{3.17}$$

From (3.17), the precise sense of the weak continuity is obvious: jumps of the normal components of $\mathbf{u}_h$ are orthogonal on g to the polynomials contained in $M_H(g)$. This in particular allows us to define a function $F \in M_H$ such that

$$F|_{\Gamma_{i,j}} := P_{M_H}((\mathbf{u}_h|_{\Omega_i} \cdot \mathbf{n}_\Gamma)|_{\Gamma_{i,j}}) = P_{M_H}((\mathbf{u}_h|_{\Omega_j} \cdot \mathbf{n}_\Gamma)|_{\Gamma_{i,j}}) \qquad i,j \in \{1,\dots,n\}. \tag{3.18}$$

Finally, using the weak continuity, we also clearly have

$$\begin{gathered} \langle \mathbf{u}_h|_{\Omega_i} \cdot \mathbf{n}_g, 1 \rangle_g = \langle \mathbf{u}_h|_{\Omega_j} \cdot \mathbf{n}_g, 1 \rangle_g = \langle \{\!\{ \mathbf{u}_h \cdot \mathbf{n}_g \}\!\}, 1 \rangle_g = \langle F, 1 \rangle_g \\ \forall g \in \mathcal{G}_{H,i,j},\ i,j \in \{1,\dots,n\}. \end{gathered} \tag{3.19}$$

3.3.1. Construction of s_h. We propose here a particular construction relying on the mesh $\widehat{\mathcal{T}}_h$; other constructions, only using the mesh $\mathcal{T}_h$, are possible.

Recall that $\widehat{\mathcal{T}}_h$ is the matching submesh of $\mathcal{T}_h$ introduced in Section 2.1 and note that $\mathbb{R}_r(\mathcal{T}_h) \subset \mathbb{R}_{r'}(\widehat{\mathcal{T}}_h)$, $r' \geq r$, i.e., every piecewise polynomial on $\mathcal{T}_h$ is also a piecewise polynomial on $\widehat{\mathcal{T}}_h$, where possibly the polynomial degree r is increased to r'. On $\mathbb{R}_{r'}(\widehat{\mathcal{T}}_h)$, we can thus use the averaging interpolate $\mathcal{I}_{\mathrm{av}} : \mathbb{R}_{r'}(\widehat{\mathcal{T}}_h) \to \mathbb{R}_{r'}(\widehat{\mathcal{T}}_h) \cap H_0^1(\Omega)$ defined as follows: for a function $\varphi_h \in \mathbb{R}_{r'}(\widehat{\mathcal{T}}_h)$, the values of $\mathcal{I}_{\mathrm{av}}(\varphi_h)$ at a Lagrange node V inside Ω are given by the average of the values of φ_h at this node,

$$\mathcal{I}_{\mathrm{av}}(\varphi_h)(V) = \frac{1}{|\widehat{\mathcal{T}}_V|} \sum_{T \in \widehat{\mathcal{T}}_V} \varphi_h|_T(V),$$

where $\widehat{\mathcal{T}}_V$ is the set of those $T \in \widehat{\mathcal{T}}_h$ to which V belongs and where for any set S, $|S|$ denotes its cardinality. Note that $\mathcal{I}_{\mathrm{av}}(\varphi_h)(V) = \varphi(V)$ at those nodes V lying in the interior of some $T \in \widehat{\mathcal{T}}_h$. At boundary nodes, the value of $\mathcal{I}_{\mathrm{av}}(\varphi_h)$ is set to zero. We refer to [21, 12, 31] for more details.

3.3.2. Construction of $\mathbf{t}_h \in \mathbf{V}_{\widehat{h}}$ by direct prescription. We define here $\mathbf{t}_h \in \mathbf{V}_{\widehat{h}}$ where $\widehat{\mathcal{T}}_h$ is the mesh introduced in Section 2.1, cf. Figure 2.2 (left).

Remark that $\{\!\{ \mathbf{u}_h \cdot \mathbf{n}_e \}\!\}$ is univalued and is a polynomial on all $e \in \widehat{\mathcal{E}}_h$. This follows from the assumption that $\widehat{\mathcal{T}}_h$ is a refinement of $\mathcal{T}_h$ and, consequently, all sides $e \in \widehat{\mathcal{E}}_h$ either coincide with the sides of $\mathcal{E}_h$, are subsides of the sides of $\mathcal{E}_h$, or pass through

the interior of some $T \in \mathcal{T}_h$. Recall also that by assumption, $\widehat{\mathcal{T}}_h$ is a matching mesh of Ω. The flux $\mathbf{t}_h$ is prescribed by the degrees of freedom of $\mathbf{V}_{\widehat{h}}$ on the mesh $\widehat{\mathcal{T}}_h$ by

$$\mathbf{t}_h \cdot \mathbf{n}_e := \{\!\{\mathbf{u}_h \cdot \mathbf{n}_e\}\!\} \qquad \forall e \in \widehat{\mathcal{E}}_h, \tag{3.20a}$$

$$(\mathbf{t}_h, \mathbf{r}_h)_T = (\mathbf{u}_h, \mathbf{r}_h)_T \qquad \forall \mathbf{r}_h \in \mathbb{R}_{l-1,*,d}(T),\ \forall T \in \widehat{\mathcal{T}}_h, \tag{3.20b}$$

where $l = k$ or k', depending on the order k or k' of $\mathbf{V}_{\widehat{h}}(T)$. Remark that $\mathbf{t}_h$ given by (3.20a)–(3.20b) indeed satisfies $\mathbf{t}_h \in \mathbf{H}(\mathrm{div}, \Omega)$, as required in Theorems 3.3 and 3.5. Recall also that by assumption, the mesh $\widehat{\mathcal{T}}_h$ only differs from the mesh $\mathcal{T}_h$ near the interface Γ. Consequently, by the above construction, $\mathbf{t}_h$ completely coincides with $\mathbf{u}_h$ on those elements T of $\widehat{\mathcal{T}}_h$ which do not share a node with Γ and the estimator $\tilde{\eta}_{\mathrm{M},T}$ given by (3.7) is equal to 0 on such T.

To apply Theorems 3.3 and 3.5, we still need to identify a partition $\mathcal{T}_H$ such that the local conservation property (3.4) holds. For a fixed Ω_i, we will form two groups of elements of $\mathcal{T}_{H,i}$, denoted respectively by $\mathcal{T}_{H,i}^{\Gamma}$ and $\mathcal{T}_{H,i}^{\mathrm{int}}$. Elements T of $\mathcal{T}_{H,i}^{\Gamma}$ are given as unions of the elements of $\widehat{\mathcal{T}}_{h,i}$ sharing a node with Γ, in a way that $\partial T \cap \Gamma_i$ is a union of sides $g \in \mathcal{G}_{H,i}$. Optimally, $\partial T \cap \Gamma_i$ is just one side $g \in \mathcal{G}_{H,i}$ for each $T \in \mathcal{T}_{H,i}^{\Gamma}$. Clearly, by (3.20a), (3.19), Green's theorem, and Assumption 3.1 (2), (3.4) on all such T follows. The elements of the second group $\mathcal{T}_{H,i}^{\mathrm{int}}$ are given directly by the elements of $\mathcal{T}_{h,i}$; consequently, (3.4) follows immediately from Assumption 3.1 (2). Denote $\mathcal{T}_H := \cup_{1\le i\le n}\mathcal{T}_{H,i}$, $\mathcal{T}_H^{\Gamma} := \cup_{1\le i\le n}\mathcal{T}_{H,i}^{\Gamma}$, and $\mathcal{T}_H^{\mathrm{int}} := \cup_{1\le i\le n}\mathcal{T}_{H,i}^{\mathrm{int}}$. The resulting mesh $\mathcal{T}_H$ can be nonmatching and needs not be shape-regular, cf. Figure 2.2 (middle). In order to optimally bound the constant $C_{\mathrm{P},T}$ from Poincaré's inequality (2.8), which is used on elements $T \in \mathcal{T}_H$, cf. (3.6), it is however preferable when the elements $T \in \mathcal{T}_H$ are convex; modifications of $\mathcal{T}_H$ to a mesh like that in Figure 2.2 (right) are possible.

REMARK 3.10 ($\mathbf{t}_h$ given by (3.20a)–(3.20b)). *The definition of* $\mathbf{t}_h$ *by* (3.20a)–(3.20b) *gives a lower-order (*k*-th or* k'*-th order RTN) polynomial* $\mathbf{t}_h$ *and is virtually cost-free as no local linear systems are to be solved. We obtain local conservation on the mesh* $\mathcal{T}_H$ *in the sense of* (3.4)*. This mesh is, however, rather unconventional and can be nonmatching and not shape-regular. Most importantly, the mortar error is only evaluated in the* h*-distance from the interface* Γ*, which, as we will see in Theorem 4.5 below, leads to its increased overestimation in the multiscale setting when* $h \ll H$*.*

3.3.3. Construction of $\mathbf{t}_h \in \mathbf{V}_{\widehat{h}}$ by the solution of h-grid-size k-th order local Neumann problems. We define here $\mathbf{t}_h \in \mathbf{V}_{\widehat{h}}$ such that $\nabla\cdot\mathbf{t}_h = P_{W_{\widehat{h}}}(f)$. We first form a partition $\mathcal{T}_H$ as in Section 3.3.2, while however, forming $\mathcal{T}_H^{\Gamma}$ by all those elements of $\widehat{\mathcal{T}}_h$ which are located in a band of width H around the interface Γ. In this way, $\mathcal{T}_H$ can be nonmatching but is shape-regular, cf. Figure 2.3 (left).

On the elements T from $\mathcal{T}_H^{\mathrm{int}}$, i.e., on those from partition $\mathcal{T}_h$, we simply set

$$\mathbf{t}_h|_T := \mathbf{u}_h|_T \qquad T \in \mathcal{T}_H^{\mathrm{int}}. \tag{3.21}$$

On the elements $T \in \mathcal{T}_H^{\Gamma}$ we consider the mesh $\widehat{\mathcal{T}}_h|_T$. On this mesh, we will, following [16], solve local Neumann problems by means of a k-th order mixed finite element method. Denote by $\mathbf{V}_{\widehat{h},\{\!\{\mathbf{u}_h\cdot\mathbf{n}_T\}\!\},T}$ the space of such $\mathbf{v}_h \in \mathbf{V}_{\widehat{h}}(T)$ that $\mathbf{v}_h\cdot\mathbf{n}_T = \{\!\{\mathbf{u}_h\cdot\mathbf{n}_T\}\!\}$ on ∂T. Denote by $\mathbf{V}_{\widehat{h},0,T}$ the space of such $\mathbf{v}_h \in \mathbf{V}_{\widehat{h}}(T)$ that $\mathbf{v}_h\cdot\mathbf{n}_T = 0$ on ∂T. We look for $\mathbf{t}_h \in \mathbf{V}_{\widehat{h},\{\!\{\mathbf{u}_h\cdot\mathbf{n}_T\}\!\},T}$ and $q_h \in W_{\widehat{h}}(T)$ satisfying $(q_h, 1)_T = 0$ such that

$$(\mathbf{K}^{-1}(\mathbf{t}_h - \mathbf{u}_h), \mathbf{v}_h)_T - (q_h, \nabla\cdot\mathbf{v}_h)_T = 0 \qquad \forall\, \mathbf{v}_h \in \mathbf{V}_{\widehat{h},0,T}, \tag{3.22a}$$

$$(\nabla\cdot\mathbf{t}_h, w_h)_T = (f, w_h)_T \qquad \forall w_h \in W_{\widehat{h}}(T) \text{ such that } (w_h, 1)_T = 0. \tag{3.22b}$$

Recall from [16] that letting $\mathbf{t}_h' := \mathbf{t}_h - \mathbf{u}_h$, $(\mathbf{t}_h', q_h)$ corresponds to the mixed finite element approximation to the local Neumann problem on T

$$-\nabla\cdot(\mathbf{K}\nabla q) = f - \nabla\cdot\mathbf{u}_h \qquad \text{in } T, \tag{3.23a}$$

$$-\mathbf{K}\nabla q\cdot\mathbf{n}_T = -\omega_g[\![\mathbf{u}_h\cdot\mathbf{n}_g]\!] \qquad \text{on all } g\in\mathcal{G}_T, \tag{3.23b}$$

$$(q,1)_T = 0, \tag{3.23c}$$

where $\omega_g := \frac{1}{2}$ when $g\not\subset\partial\Omega$ and $\omega_g := 0$ when $g\subset\partial\Omega$. Note that these problems are well-posed as the Neumann boundary conditions are in equilibrium with the load,

$$\sum_{g\in\mathcal{G}_T}\langle\mathbf{u}_h\cdot\mathbf{n}_T - \omega_g[\![\mathbf{u}_h\cdot\mathbf{n}_g]\!],1\rangle_g = \langle\{\!\{\mathbf{u}_h\cdot\mathbf{n}_T\}\!\},1\rangle_{\partial T} = (f,1)_T.$$

This follows by (3.19), Green's theorem, and Assumption 3.1 (2). Note also that indeed $\mathbf{t}_h$ given by (3.22a)–(3.22b) is in $\mathbf{V}_{\widehat{h}}$, as the Neumann boundary condition on $T\in\mathcal{T}_H^\Gamma$ given by $\{\!\{\mathbf{u}_h\cdot\mathbf{n}_T\}\!\}$ gives the continuity of the normal component of $\mathbf{t}_h$ on $\partial T\cap\Gamma$ (the same condition is imposed from the opposite side), as well as on $\partial T\setminus\Gamma$, where $\{\!\{\mathbf{u}_h\cdot\mathbf{n}_T\}\!\} = \mathbf{u}_h\cdot\mathbf{n}_T$, which is the value imposed in (3.21) on $T\in\mathcal{T}_H^{\mathrm{int}}$. Finally, as the mixed finite element method minimizes the complementary energy, another way to rewrite equivalently (3.22a)–(3.22b) is

$$\mathbf{t}_h|_T = \arg\inf_{\mathbf{v}_h\in\mathbf{V}_{\widehat{h},\{\!\{\mathbf{u}_h\cdot\mathbf{n}_T\}\!\},T},\ \nabla\cdot\mathbf{v}_h = P_{W_{\widehat{h}}}(f)} |||\mathbf{u}_h-\mathbf{v}_h|||_{*,T}.$$

Thus, on each $T\in\mathcal{T}_H$, $\mathbf{t}_h$ is the best choice from the space $\mathbf{V}_{\widehat{h},\{\!\{\mathbf{u}_h\cdot\mathbf{n}_T\}\!\},T}$ to minimize the quantity $|||\mathbf{u}_h-\mathbf{v}_h|||_{*,T}$ (subject to the constraint $\nabla\cdot\mathbf{v}_h = P_{W_{\widehat{h}}}(f)$). Remark that this quantity is related to the definition of the $\tilde{\eta}_{\mathrm{M},T}$ estimator, see (3.7).

REMARK 3.11 ($\mathbf{t}_h$ given by (3.21)–(3.22b)). *The definition* (3.21)–(3.22b) *gives a lower-order (k-th order RTN) polynomial* $\mathbf{t}_h$ *and is moderately expensive as local linear systems need to be solved. These systems correspond to mixed finite element approximations of order k posed over H-sized subdomains with h-sized grids. We obtain local conservation on the fine mesh* $\widehat{\mathcal{T}}_h$ *in the sense of* (3.12). *Consequently, we can use* (3.13) *instead of* (3.6). *The mesh* $\mathcal{T}_H$ *is here nonmatching but shape-regular and only serves for the computation of the flux* $\mathbf{t}_h$ *and not for the evaluation of the estimates of Sections 3.1–3.2. The mortar error is evaluated in the H-distance from the interface* Γ. *As we will see in Theorem 4.5 below, this leads to a smaller overestimation in the multiscale setting when* $h\ll H$, *in comparison with the estimator* η_{M} *of* (3.3) *or with* (3.7) *evaluated using* $\mathbf{t}_h$ *of Section 3.3.2.*

3.3.4. Construction of $\mathbf{t}_h\in\mathbf{V}_H$ by the solution of H-grid-size m-th order local Neumann problems. We define here the flux which is of higher-order (m-th order RTN) on the coarse mesh $\mathcal{T}_H$, $\mathbf{t}_h\in\mathbf{V}_H$. For this purpose, we need $\mathcal{T}_H$ to be both matching and shape-regular; the elements of $\mathcal{T}_H^{\mathrm{int}}$ are no more given by the elements of $\mathcal{T}_h$ but rather by unions of elements of $\mathcal{T}_h$ as for $\mathcal{T}_H^\Gamma$, cf. Figure 2.3 (right). Recall that the main requirement on $\mathcal{T}_H$ is that the restriction of $\mathcal{T}_H$ on Γ is the interface mesh $\mathcal{G}_H$.

In this section, we extend the mesh $\mathcal{G}_H$ from the interface Γ only to $\Gamma\cup\partial\Omega$; we define $\mathcal{G}_H$ on $\partial\Omega$ by the sides of $\mathcal{T}_H$ lying in $\partial\Omega$. We also suppose that the mortar space M_H is defined over the whole new $\mathcal{G}_H$ with the same m-th order polynomials. Let the flux function F be on Γ given by (3.18). We extend it on $\partial\Omega$ by

$$F|_{\partial\Omega} := P_{M_H}((\mathbf{u}_h\cdot\mathbf{n}_\Omega)|_{\partial\Omega}).$$

Consider a fixed Ω_i and the mesh $\mathcal{T}_{H,i}$. We solve local Neumann problems by means of a m-th order mixed finite element method. Denote by $\mathbf{V}_{H,F,\Omega_i}$ the space of such $\mathbf{v}_H \in \mathbf{V}_H(\Omega_i)$ that $\mathbf{v}_H{\cdot}\mathbf{n}_\Gamma = F$ on $\partial\Omega_i \cap \Gamma$ and that $\mathbf{v}_H{\cdot}\mathbf{n}_{\Omega_i} = F$ on $\partial\Omega_i \cap \partial\Omega$ and by $\mathbf{V}_{H,0,\Omega_i}$ the space of such $\mathbf{v}_H \in \mathbf{V}_H(\Omega_i)$ that $\mathbf{v}_H{\cdot}\mathbf{n}_{\Omega_i} = 0$ on $\partial\Omega_i$. We look for $\mathbf{t}_h \in \mathbf{V}_{H,F,\Omega_i}$ and $q_H \in W_H(\Omega_i)$ satisfying $(q_H, 1)_{\Omega_i} = 0$ such that

$$(\mathbf{K}^{-1}(\mathbf{t}_h - \mathbf{u}_h), \mathbf{v}_H)_{\Omega_i} - (q_H, \nabla{\cdot}\mathbf{v}_H)_{\Omega_i} = 0 \qquad \forall\, \mathbf{v}_H \in \mathbf{V}_{H,0,\Omega_i}, \tag{3.24a}$$

$$(\nabla{\cdot}\mathbf{t}_h, w_H)_{\Omega_i} = (f, w_H)_{\Omega_i} \qquad \forall w_H \in W_H(\Omega_i) \text{ such that } (w_H, 1)_{\Omega_i} = 0. \tag{3.24b}$$

Once again, these problems are well-posed as

$$\langle F\mathbf{n}_{\Omega_i}{\cdot}\mathbf{n}_\Gamma, 1\rangle_{\partial\Omega_i\cap\Gamma} + \langle F, 1\rangle_{\partial\Omega_i\cap\partial\Omega} = (f, 1)_{\Omega_i}$$

by the same reasoning as in the previous sections. We also indeed have $\mathbf{t}_h \in \mathbf{V}_H$, as the Neumann boundary condition on Γ given by F gives the continuity of the normal component of $\mathbf{t}_h$. Finally, as above, (3.24a)–(3.24b) is equivalent to

$$\mathbf{t}_h|_T = \arg \inf_{\mathbf{v}_H \in \mathbf{V}_{H,F,\Omega_i},\, \nabla\cdot\mathbf{v}_H = P_{W_H}(f)} |||\mathbf{u}_h - \mathbf{v}_H|||_{*,\Omega_i}. \tag{3.25}$$

REMARK 3.12 ($\mathbf{t}_h$ given by (3.24a)–(3.24b)). *The definition* (3.24a)–(3.24b) *gives a higher-order (m-th order RTN) polynomial* $\mathbf{t}_h$ *and is more expensive with semi-local linear systems. These systems correspond to mixed finite element approximations of order m posed over the subdomains* Ω_i *with H-sized grids. We obtain local conservation on the mesh* $\mathcal{T}_H$ *in the sense of* (3.14)*. Consequently,* (3.6) *takes the form* (3.15)*. The mesh* $\mathcal{T}_H$ *is here both matching and shape-regular. The mortar error is evaluated in the* Ω_i*-size-distance from the interface* Γ*, which, as we will see in Theorem 4.5 below, leads to its optimal estimation in the multiscale setting when* $h \ll H$*.*

4. Local efficiency of the a posteriori estimates. We state here the local efficiency of the estimators of Theorems 3.2–3.5. We suppose for simplicity that f is a piecewise polynomial of degree q.

We will need the following assumption:

ASSUMPTION 4.1 (Properties of $\tilde{p}_h$). *Let*

1. $\tilde{p}_h \in \mathbb{R}_r(\mathcal{T}_h)$ *for some* $r \geq 1$,
2. $\langle [\![\tilde{p}_h]\!], 1\rangle_e = 0 \qquad \forall e \in \mathcal{E}_h^{\rm int} \cup \mathcal{E}_h^{\rm ext}$,
3. $\langle [\![\tilde{p}_h]\!], 1\rangle_g = 0 \qquad \forall g \in \mathcal{G}_h^*$.

Assumption 4.1 means that $\tilde{p}_h$ is a piecewise polynomial, that the means of traces on interior sides in each subdomain are continuous, that the means of traces on boundary sides are zero, and that the means of traces on collections of sides inside the interface Γ are continuous. For all the results, we assume Assumption 4.1 (1). This assumption is satisfied by all usual numerical methods. We will present some results without Assumptions 4.1 (2)–(3), as these assumptions are not satisfied by all numerical methods.

The following theorem gives the efficiency for the estimator $\eta_{{\rm DF},T}$ and shows that the efficiency of the estimators $\eta_{{\rm P},T}$ and $\eta_{{\rm DFM},T}$ is controlled by the efficiency of the estimators $\eta_{{\rm DF},T}$, $\eta_{{\rm NC},T}$, and $\tilde{\eta}_{{\rm M},T}$.

THEOREM 4.2 (Local efficiency of the diffusive flux and potential estimators). *Let* $\tilde{p}_h \in H^1(\mathcal{T}_h)$, $\mathbf{u}_h \in \mathbf{L}^2(\Omega)$, $s_h \in H_0^1(\Omega)$, *and* $\mathbf{t}_h \in \mathbf{H}(\mathrm{div}, \Omega)$ *be arbitrary. Then, for all* $T \in \mathcal{T}_h$*,*

$$\begin{aligned}
\eta_{{\rm DF},T} &\leq |||\mathbf{u} - \mathbf{u}_h|||_{*,T} + |||p - \tilde{p}_h|||_T,\\
\eta_{{\rm P},T} &\leq \eta_{{\rm DF},T} + \eta_{{\rm NC},T},\\
\eta_{{\rm DFM},T} &\leq \eta_{{\rm DF},T} + \tilde{\eta}_{{\rm M},T}.
\end{aligned}$$

We will henceforth assume that the mesh families $\{\mathcal{T}_h\}_{h>0}$ and $\{\widehat{\mathcal{T}}_h\}_{h>0}$ are shape-regular in the sense that there exist constants $\kappa_{\mathcal{T}_h} > 0$ and $\kappa_{\widehat{\mathcal{T}}_h} > 0$ such that $\min_{T\in\mathcal{T}_h} \rho_T/h_T \geq \kappa_{\mathcal{T}_h}$ and $\min_{T\in\widehat{\mathcal{T}}_h} \rho_T/h_T \geq \kappa_{\widehat{\mathcal{T}}_h}$ for all $h > 0$, where ρ_T denotes the diameter of the largest ball inscribed in T. For the approach of Section 3.3.4, we will also assume that $\{\mathcal{T}_H\}_{H>0}$ are shape-regular, i.e., that there exists a constant $\kappa_{\mathcal{T}_H} > 0$ such that $\min_{T\in\mathcal{T}_H} \rho_T/H_T \geq \kappa_{\mathcal{T}_H}$ for all $H > 0$. We will in the sequel use the notation $A \lesssim B$ to denote that $A \leq CB$, where the constant C depends on the space dimension d, the polynomial degree r of $\tilde{p}_h$, r' of s_h, k of $\mathbf{u}_h$, k, k', or m of $\mathbf{t}_h$, and q of f, on the shape regularity parameters $\kappa_{\mathcal{T}_h}$ of $\mathcal{T}_h$, $\kappa_{\widehat{\mathcal{T}}_h}$ of $\widehat{\mathcal{T}}_h$, (and $\kappa_{\mathcal{T}_H}$ of $\mathcal{T}_H$), on $\mathbf{K}$, and on the constant $C_{\mathcal{G}_h^*}$ from (2.1) but is independent of any mesh size, the domain Ω, and the regularity of the weak solution $(p, \mathbf{u})$. Let, for $T \in \mathcal{T}_h$, the notation $\mathfrak{T}_T$ stand for the union of all elements $T' \in \mathcal{T}_h$ sharing a node with T and $\mathfrak{T}_{T,\Gamma}$ for the union of all elements $T' \in \mathcal{T}_h$ sharing a node with T or with that $g \in \mathcal{G}_h^*$ which contains a node of T. Similarly, for $T \in \mathcal{T}_H$, let the notation $\mathfrak{T}_{T,\Gamma}$ stand for the union of all elements $T' \in \mathcal{T}_h$ sharing a node with that $g \in \mathcal{G}_H$ which contains a side of T and set $h_{\mathfrak{T}_{T,\Gamma}} := \min_{T'\in\mathfrak{T}_{T,\Gamma}} h_{T'}$. We also denote by $\mathfrak{T}_g$ all the elements of $\mathcal{T}_h$ which share a node with a given $g \in \mathcal{G}_H$ and set $h_{\mathfrak{T}_g} := \min_{T\in\mathfrak{T}_g} h_T$.

The following theorem is based on the entire Assumption 4.1:

THEOREM 4.3 (Local efficiency of the nonconformity estimator). *Let Assumption 4.1 hold and let $s_h \in \mathbb{R}_{r'}(\widehat{\mathcal{T}}_h)$ be given by $s_h := \mathcal{I}_{\rm av}(\tilde{p}_h)$. Then, for all $T \in \mathcal{T}_h$,*

$$\eta_{{\rm NC},T} \lesssim |||p - \tilde{p}_h|||_{\mathfrak{T}_T} \qquad \text{if } T \cap \Gamma = \emptyset, \tag{4.1a}$$

$$\eta_{{\rm NC},T} \lesssim |||p - \tilde{p}_h|||_{\mathfrak{T}_{T,\Gamma}} \qquad \text{if } T \cap \Gamma \neq \emptyset. \tag{4.1b}$$

For the following theorem, Assumption 4.1 (1) is sufficient:

THEOREM 4.4 (Local efficiency of the nonconformity estimator). *Let Assumption 4.1 (1) hold and let $s_h \in \mathbb{R}_{r'}(\widehat{\mathcal{T}}_h)$ be given by $s_h := \mathcal{I}_{\rm av}(\tilde{p}_h)$. Then, for all $T \in \mathcal{T}_h$,*

$$\eta_{{\rm NC},T} \lesssim \sum_{e\in\widehat{\mathcal{E}}_h;\, e\cap T\neq\emptyset} h_e^{-\frac{1}{2}} \|[\![\tilde{p}_h]\!]\|_e. \tag{4.2a}$$

The following theorem hinges on Assumption 3.1:

THEOREM 4.5 (Local efficiency of the residual and mortar estimators). *Let Assumption 3.1 be satisfied. Then:*

1) Case where $\eta_{{\rm R},h}$ is given by (3.2) and $\eta_{\rm M}$ by (3.3), localized by (3.16).

Let $T \in \mathcal{T}_h$ and $g \in \mathcal{G}_H$. Then

$$\eta_{{\rm R},h,T} \lesssim |||\mathbf{u} - \mathbf{u}_h|||_{*,T}, \tag{4.3a}$$

$$\eta_{{\rm M},g} \lesssim \sqrt{\frac{H_g}{h_{\mathfrak{T}_g}}} |||\mathbf{u} - \mathbf{u}_h|||_{*,\mathfrak{T}_g}. \tag{4.3b}$$

2) Case where $\mathbf{t}_h$ is constructed following Section 3.3.2, $\eta_{{\rm R},H,T}$ is given by (3.6), and $\tilde{\eta}_{\rm M}$ by (3.7).

Let $T \in \mathcal{T}_h \cap \mathcal{T}_H^{\rm int}$. Then

$$\eta_{{\rm R},H,T} \lesssim |||\mathbf{u} - \mathbf{u}_h|||_{*,T}, \tag{4.4a}$$

$$\tilde{\eta}_{{\rm M},T} = 0. \tag{4.4b}$$

Let $T \in \mathcal{T}_h$, $T \subset T'$ for some $T' \in \mathcal{T}_H^\Gamma$. Then

$$\eta_{\mathrm{R},H,T} \lesssim \frac{H_{T'}}{h_T} |||\mathbf{u} - \mathbf{u}_h|||_{*,\mathfrak{T}_T}, \tag{4.5a}$$

$$\tilde{\eta}_{\mathrm{M},T} \lesssim |||\mathbf{u} - \mathbf{u}_h|||_{*,\mathfrak{T}_T}. \tag{4.5b}$$

3) Case where $\mathbf{t}_h$ is constructed following Section 3.3.3, $\eta_{\mathrm{R},H}$ takes the form $\eta_{\mathrm{R},\widehat{h}}$ of (3.13), and $\tilde{\eta}_{\mathrm{M}}$ is given by (3.7).

Let $T \in \widehat{\mathcal{T}}_h$. Then

$$\eta_{\mathrm{R},\widehat{h},T} \lesssim |||\mathbf{u} - \mathbf{u}_h|||_{*,T}. \tag{4.6}$$

Let $T \in \mathcal{T}_H^{\mathrm{int}}$. Then

$$\tilde{\eta}_{\mathrm{M},T} = 0. \tag{4.7}$$

Let $T' \in \mathcal{T}_H^\Gamma$. Suppose here additionally that $f \in \mathbb{R}_k(\mathcal{T}_h)$ and that $\nabla{\cdot}\mathbf{u}_h = P_{W_h}(f)$ so that $f - \nabla{\cdot}\mathbf{u}_h = 0$. Then

$$\tilde{\eta}_{\mathrm{M},T'} \lesssim \sqrt{\frac{H_{T'}}{h_{\mathfrak{T}_{T',\Gamma}}}} |||\mathbf{u} - \mathbf{u}_h|||_{*,\mathfrak{T}_{T',\Gamma}}. \tag{4.8}$$

4) Case where $\mathbf{t}_h$ is constructed following Section 3.3.4, $\eta_{\mathrm{R},H}$ takes the form (3.15), and $\tilde{\eta}_{\mathrm{M}}$ is given by (3.7).

Assume that $\{\mathcal{T}_H\}_{H>0}$ are shape-regular. Assume also sufficient smoothness leading to (7.5), see Section 7 below. Let $T' \in \mathcal{T}_H$ and let $i \in \{1, \dots, n\}$. Then

$$\eta_{\mathrm{R},H,T'} \lesssim (\tilde{\eta}_{\mathrm{M},T'} + |||\mathbf{u} - \mathbf{u}_h|||_{T'}), \tag{4.9a}$$

$$\tilde{\eta}_{\mathrm{M},\Omega_i} \leq |||\mathbf{u}_h - \mathbf{u}|||_{*,\Omega_i} + \eta_{\mathrm{R},h,\Omega_i} + CH^{m+1}. \tag{4.9b}$$

REMARK 4.6 (Efficiency of η_{NC}). *Theorems 4.3 and 4.4 show that Assumptions 4.1 (2)–(3) are necessary in order to obtain local efficiency of the nonconformity estimator η_{NC}. This fact has been previously employed in, e.g., [2, 3, 30, 33] in the non-multiscale setting. We show below that the multiscale mortar mixed finite element method of [6] satisfies Assumptions 4.1 (2)–(3). In order to obtain two-sided bounds in the same norm when Assumptions 4.1 (2)–(3) are not satisfied, one could, noticing that $[\![\tilde{p}_h]\!] = [\![\tilde{p}_h - p]\!]$ for all $e \in \widehat{\mathcal{E}}_h$, add $\sum_{e \in \widehat{\mathcal{E}}_h} h_e^{-\frac{1}{2}} \|[\![\tilde{p}_h]\!]\|_e$ to both the error and estimate, as usually done in the discontinuous Galerkin method.*

REMARK 4.7 (Higher-order convergence of $\eta_{\mathrm{R},h}$, $\eta_{\mathrm{R},\widehat{h}}$, and $\eta_{\mathrm{R},H}$). *The residual a posteriori error estimate $\eta_{\mathrm{R},\widehat{h}}$ given by (3.13) represents a higher-order convergent ("data oscillation") term whenever $f \in H^{k+1}(\widehat{\mathcal{T}}_h)$. It in fact vanishes whenever $f \in \mathbb{R}_k(\widehat{\mathcal{T}}_h)$. A similar remark holds for $\eta_{\mathrm{R},H}$ taking the form (3.15) and also for $\eta_{\mathrm{R},h}$ given by (3.2) whenever $\nabla{\cdot}\mathbf{u}_h = P_{W_h}(f)$.*

REMARK 4.8 ((Semi-)robustness with respect to inhomogeneities and anisotropies in $\mathbf{K}$). *The constants in the above inequalities depend on local inhomogeneities and anisotropies in $\mathbf{K}$ in the same way as in [33], so that the estimates are semi-robust with respect to $\mathbf{K}$. Replacing the energy (semi-)norms $|||\cdot|||$ and $|||\cdot|||_*$ of (2.6)–(2.7) by dual norms as in [32], global efficiency and full robustness with respect to the inhomogeneities and anisotropies in $\mathbf{K}$ can be shown.*

REMARK 4.9 (Robustness with respect to the ratio H/h). *As the results of Theorem 4.3 show, the nonconformity estimator η_{NC} leads under Assumptions 4.1 (2)–(3)*

to the overestimation factor independent of the ratio H/h, i.e., to the robustness with respect to multiscale. These conditions are shown below to be verified by the multiscale mortar mixed finite element method of [6]. According to Theorem 4.5, neither of the flux reconstruction of Sections 3.3.2 or 3.3.3 leads to a similar robustness result. A different situation appears to arise using the reconstruction of Section 3.3.4. The a priori error estimates presented in [6] for the multiscale mortar mixed finite element method indicate that in that case, $|||\mathbf{u}_h - \mathbf{u}|||_*$ converges as $\mathcal{O}(H^{m+\frac{1}{2}})$, so that CH^{m+1} is of higher order. This result is of course not perfect as it hinges on the high regularity of the exact solution and, moreover, the lower bound (4.9b) features the factor CH^{m+1} on the right-hand-side, but it shows robustness with respect to the ratio H/h. This is confirmed by the numerical experiments carried out in Section 8 below.

5. Multiscale, multinumerics, and mortar discretizations. We present here different methods that fit into the framework of the previous sections. In order to check that the presented a posteriori error estimates and their efficiency hold true, we only need to verify that Assumptions 3.1 and 4.1 (1) are satisfied. Additionally, Assumption 4.1 (2)–(3) will also be satisfied in the first case below.

5.1. Multiscale mortar mixed finite element method. The multiscale mortar mixed finite element method for the problem (1.1a)–(1.1b), see [6], reads: for $k \geq 0$, find $\mathbf{u}_h \in \mathbf{V}_h$, $p_h \in W_h$, and $\lambda_H \in M_H$ such that,

$$(\mathbf{K}^{-1}\mathbf{u}_h, \mathbf{v}_h)_{\Omega_i} - (p_h, \nabla\cdot\mathbf{v}_h)_{\Omega_i} + \langle \lambda_H, \mathbf{v}_h\cdot\mathbf{n}_{\Omega_i}\rangle_{\Gamma_i} = 0 \quad \forall\, \mathbf{v}_h \in \mathbf{V}_{h,i},\ \forall i, \tag{5.1a}$$

$$(\nabla\cdot\mathbf{u}_h, w_h)_{\Omega_i} = (f, w_h)_{\Omega_i} \qquad \forall w_h \in W_{h,i},\ \forall i, \tag{5.1b}$$

$$\sum_{i=1}^{n} \langle \mathbf{u}_h\cdot\mathbf{n}_{\Omega_i}, \mu_H\rangle_{\Gamma_i} = 0 \qquad \forall \mu_H \in M_H. \tag{5.1c}$$

Thus $\mathbf{u}_h$ satisfying Assumption 3.1 is directly given in the multiscale mortar mixed finite element method. The p_h obtained directly from (5.1a)–(5.1c) is not suitable to be used as $\tilde{p}_h$ in the a posteriori framework of Sections 3–4, see the discussion in [30, 33]. We devote the rest of this section to obtaining a suitable $\tilde{p}_h$.

Let $\Lambda_{h,i}$ be the usual Lagrange multiplier spaces associated with $\mathbf{V}_{h,i} \times W_{h,i}$, see [11, 28], and let $\tilde{\mathbf{V}}_{h,i}$ be the spaces without the interelement constraints, $\tilde{\mathbf{V}}_{h,i} := \bigoplus_{T\in\mathcal{T}_{h,i}} \mathbf{V}_{h,i}(T)$. Set $\Lambda_h := \bigoplus_{i=1}^n \Lambda_{h,i}$, $\tilde{\mathbf{V}}_h := \bigoplus_{i=1}^n \tilde{\mathbf{V}}_{h,i}$. Let $\mathbf{u}_h$, p_h be the solution of (5.1a)–(5.1c). We define $\lambda_h \in \Lambda_h$ by

$$\langle \lambda_h, \mathbf{v}_e\cdot\mathbf{n}_T\rangle_e := -(\mathbf{K}^{-1}\mathbf{u}_h, \mathbf{v}_e)_T + (p_h, \nabla\cdot\mathbf{v}_e)_T \tag{5.2}$$

for all flux basis functions $\mathbf{v}_e$ of $\tilde{\mathbf{V}}_{h,i}$ associated with the element $T \in \mathcal{T}_h$ and its side e. Let $P_{\tilde{\mathbf{V}}_h}$ be the $\mathbf{L}^2(\Omega)$-orthogonal projection onto $\tilde{\mathbf{V}}_h$ with respect to the scalar product $(\mathbf{K}^{-1}\cdot,\cdot)$ and P_{Λ_h} the $L^2(\mathcal{E}_h^{\mathrm{int},\Gamma})$-orthogonal projection onto Λ_h, i.e.,

$$P_{\tilde{\mathbf{V}}_h} : \mathbf{L}^2(\Omega) \to \tilde{\mathbf{V}}_h \quad \text{for } \mathbf{v} \in \mathbf{L}^2(\Omega), \quad (\mathbf{K}^{-1}(\mathbf{v} - P_{\tilde{\mathbf{V}}_h}(\mathbf{v})), \mathbf{v}_h) = 0 \quad \forall \mathbf{v}_h \in \tilde{\mathbf{V}}_h,$$
$$P_{\Lambda_h} : L^2(\mathcal{E}_h^{\mathrm{int},\Gamma}) \to \Lambda_h \quad \text{for } \mu \in L^2(\mathcal{E}_h^{\mathrm{int},\Gamma}),\ (\mu - P_{\Lambda_h}(\mu), \mu_h)_{\mathcal{E}_h^{\mathrm{int},\Gamma}} = 0 \quad \forall \mu_h \in \Lambda_h.$$

Our basic tool for the a posteriori error analysis of the mixed finite element method will be the local postprocessing of the potential p_h introduced in [5], see also [30]. Let $\tilde{W}_h$ be a polynomial space of functions φ_h satisfying

$$\langle [\![\varphi_h]\!], \psi_h\rangle_e = 0 \qquad \forall e \in \mathcal{E}_h^{\mathrm{int}} \cup \mathcal{E}_h^{\mathrm{ext}},\ \forall \psi_h \in \mathbb{R}_k(e) \tag{5.4}$$

and specified in [5, 30]. Then we define:

DEFINITION 5.1 (Postprocessing $\tilde{p}_h$ of p_h). *We define* $\tilde{p}_h \in \tilde{W}_h$ *by*

$$P_{W_h}(\tilde{p}_h) = p_h, \tag{5.5a}$$

$$P_{\Lambda_h}(\tilde{p}_h) = \lambda_h. \tag{5.5b}$$

Note that employing (5.5a)–(5.5b) in (5.2) and using $\nabla{\cdot}\mathbf{V}_h(T) = W_h(T)$ and $\mathbf{V}_h(T){\cdot}\mathbf{n}_T|_{\partial T\setminus\partial\Omega} = \Lambda_h(T)$ gives, for all $T \in \mathcal{T}_h$,

$$(\mathbf{K}^{-1}\mathbf{u}_h, \mathbf{v}_h)_T - (\tilde{p}_h, \nabla{\cdot}\mathbf{v}_h)_T + \langle \tilde{p}_h, \mathbf{v}_h{\cdot}\mathbf{n}_T\rangle_{\partial T\setminus\partial\Omega} = 0 \qquad \forall\, \mathbf{v}_h \in \mathbf{V}_h(T). \tag{5.6}$$

Employing Green's theorem for the two last terms of the above expression gives

$$(\mathbf{K}^{-1}(\mathbf{u}_h + \mathbf{K}\nabla\tilde{p}_h), \mathbf{v}_h)_T = 0 \qquad \forall\, \mathbf{v}_h \in \mathbf{V}_h(T) \quad \forall T \in \mathcal{T}_h,$$

which is nothing but

$$P_{\tilde{\mathbf{V}}_h}(-\mathbf{K}\nabla\tilde{p}_h) = \mathbf{u}_h. \tag{5.7}$$

We refer to [5, 33] for more details.

The postprocessed potential $\tilde{p}_h$ satisfies Assumption 4.1 (1) as $\tilde{W}_h$ is a piecewise polynomial space. Moreover, Assumption 4.1 (2) is implied by (5.4). The following lemma shows that Assumption 4.1 (3) for the above $\tilde{p}_h$ holds as well.

LEMMA 5.2 (Weak continuity of $\tilde{p}_h$). *For any union of interface sides* $g \in \mathcal{G}_h^*$,

$$\langle [\![\tilde{p}_h]\!], \psi_h\rangle_g = 0 \qquad \forall \psi_h \in \mathbb{R}_k(g). \tag{5.8}$$

Moreover, for all $e \in \mathcal{E}_h^\Gamma$,

$$\langle \tilde{p}_h|_{T_e} - \lambda_H, \psi_h\rangle_e = 0 \qquad \forall \psi_h \in \mathbb{R}_k(e), \tag{5.9}$$

where T_e *is the element of* $\mathcal{T}_h$ *having* e *as side.*

Proof. Fix $e \in \mathcal{E}_h^\Gamma$ (recall that this also fixes the subdomain Ω_i and an element $T_e \in \mathcal{T}_{h,i}$) and take all basis functions $\mathbf{v}_e$ in (5.1a). Using (5.6) and (5.5a), this gives

$$\langle -\tilde{p}_h|_{T_e} + \lambda_H, \mathbf{v}_e{\cdot}\mathbf{n}_{T_e}\rangle_e = 0,$$

whence (5.9) follows. To prove (5.8), take any $g \in \mathcal{G}_h^*$. Thus g is given by one or more sides from some Ω_i and by one or more sides from some Ω_j; as from both subdomains, the associated basis functions fill the space $\mathbb{R}_k(g)$, (5.8) follows from (5.9). ∎

5.2. Multiscale mortar discontinuous Galerkin method. We consider here the multiscale mortar discontinuous Galerkin method of [19] for the problem (1.1a)–(1.1b). Let $\mathbf{K}$ be piecewise constant on $\mathcal{T}_h$ in this section for simplicity and let $k \geq 1$. Then the method reads: find $p_h \in W_h$ and $\lambda_H \in M_H$ such that

$$\mathcal{B}_{h,i}(p_h, \lambda_H; \varphi_h) = (f, \varphi_h)_{\Omega_i} \qquad \forall \varphi_h \in W_{h,i},\ \forall i \in \{1, \dots, n\}, \tag{5.10a}$$

$$\sum_{i=1}^{n} \sum_{g\in\mathcal{G}_{H,i}} \Big\langle -\mathbf{K}\nabla p_h|_{\Omega_i}{\cdot}\mathbf{n}_{\Omega_i} + \alpha_g \frac{\sigma_{\mathbf{K},g}}{H_g}\big(p_h|_{\Omega_i} - \pi_{k,\mathcal{E}_{h,i}^\Gamma}(\lambda_H)\big), \mu_H\Big\rangle_g = 0 \qquad \forall \mu_H \in M_H, \tag{5.10b}$$

where

$$
\begin{aligned}
\mathcal{B}_{h,i}(p_h,\lambda_H;\varphi_h) := &- \sum_{e\in\mathcal{E}_{h,i}^{\mathrm{int}}} \{\langle \{\!\{\mathbf{K}\nabla p_h\cdot\mathbf{n}_e\}\!\}, [\![\varphi_h]\!]\rangle_e + \theta\langle \{\!\{\mathbf{K}\nabla\varphi_h\cdot\mathbf{n}_e\}\!\}, [\![p_h]\!]\rangle_e\} \\
&- \sum_{g\in\mathcal{G}_{H,i}} \Big\{ \Big\langle \mathbf{K}\nabla p_h|_{\Omega_i}\cdot\mathbf{n}_{\Omega_i} - \alpha_g\frac{\sigma_{\mathbf{K},g}}{H_g}(p_h|_{\Omega_i}-\lambda_H), \varphi_h|_{\Omega_i}\Big\rangle_g \\
&+ \bar\theta\langle \mathbf{K}\nabla\varphi_h|_{\Omega_i}\cdot\mathbf{n}_{\Omega_i}, p_h|_{\Omega_i}-\lambda_H\rangle_g\Big\} \\
&+ (\mathbf{K}\nabla p_h,\nabla\varphi_h)_{\Omega_i} + \sum_{e\in\mathcal{E}_{h,i}^{\mathrm{int}}} \Big\langle \alpha_e\frac{\sigma_{\mathbf{K},e}}{h_e}[\![p_h]\!], [\![\varphi_h]\!]\Big\rangle_e .
\end{aligned}
\tag{5.11}
$$

Here α_e, $e\in\mathcal{E}_h^{\mathrm{int}}$, and α_g, $g\in\mathcal{G}_H$, are the penalty parameters (taken sufficiently large), $\sigma_{\mathbf{K},e}$ and $\sigma_{\mathbf{K},g}$ are $\mathbf{K}$-dependent weights, and $\theta\in\{-1,0,1\}$, $\bar\theta\in\{-1,0,1\}$ lead to the usual choices of the various discontinuous Galerkin schemes. For the sake of simplicity, we suppose here that $\mathcal{E}_{h,i}^{\Gamma}$ is a refinement of $\mathcal{G}_{H,i}$ for all $i\in\{1,\dots,n\}$. In fact, in comparison with [19], we have replaced in (5.10b) λ_H by $\pi_{k,\mathcal{E}_{h,i}^{\Gamma}}(\lambda_H)$ (recall that $\pi_{k,\mathcal{E}_{h,i}^{\Gamma}}$ is the L^2-orthogonal projection onto piecewise polynomials of order k on $\mathcal{E}_{h,i}^{\Gamma}$). We refer to Remark 5.5 below for the original version and to Remark 5.6 below for yet another modification. Note that as $\varphi_h\in W_{h,i}$, $\varphi_h|_{\Gamma_i}$ is a piecewise polynomial of order k on $\mathcal{E}_{h,i}^{\Gamma}$. Consequently, we can equivalently replace λ_H by $\pi_{k,\mathcal{E}_{h,i}^{\Gamma}}(\lambda_H)$ also in the fourth right-hand side term of (5.11). Note that λ_H can be equivalently replaced by $\pi_{k,\mathcal{E}_{h,i}^{\Gamma}}(\lambda_H)$ also in the multiscale mortar mixed finite element method (5.1a)–(5.1c).

Following [22, 15], we now introduce a reconstructed flux $\mathbf{u}_h$. We will use it in our a posteriori error estimates but we remind that it can be of independent interest for, e.g., subsequent contaminant transport modeling.

DEFINITION 5.3 (Discontinuous Galerkin flux reconstruction). *Let $T\in\mathcal{T}_h$. Then the reconstructed flux $\mathbf{u}_h|_T\in\mathbf{V}_h(T)$ is given by*

$$
\langle \mathbf{u}_h\cdot\mathbf{n}_e, q_h\rangle_e = \Big\langle -\{\!\{\mathbf{K}\nabla p_h\cdot\mathbf{n}_e\}\!\} + \alpha_e\frac{\sigma_{\mathbf{K},e}}{h_e}[\![p_h]\!], q_h\Big\rangle_e \qquad \forall q_h\in\mathbb{R}_k(e),\ \forall e\in\mathcal{E}_T,\ e\not\subset\Gamma, \tag{5.12a}
$$

$$
\langle \mathbf{u}_h\cdot\mathbf{n}_e, q_h\rangle_e = \Big\langle -\mathbf{K}\nabla p_h\cdot\mathbf{n}_e + \alpha_g\frac{\sigma_{\mathbf{K},g}}{H_g}(p_h-\lambda_H), q_h\Big\rangle_e \qquad \forall q_h\in\mathbb{R}_k(e),\ \forall e\in\mathcal{E}_T,\ e\subset g\in\mathcal{G}_H, \tag{5.12b}
$$

$$
\begin{aligned}
(\mathbf{u}_h,\mathbf{r}_h)_T = &-(\mathbf{K}\nabla p_h,\mathbf{r}_h)_T + \theta\sum_{e\in\mathcal{E}_T,\, e\not\subset\Gamma}\omega_e\langle \mathbf{K}\mathbf{r}_h\cdot\mathbf{n}_e, [\![p_h]\!]\rangle_e \\
&+\bar\theta\sum_{e\in\mathcal{E}_T,\, e\subset\Gamma}\langle \mathbf{K}\mathbf{r}_h\cdot\mathbf{n}_e, (p_h-\lambda_H)\mathbf{n}_T\cdot\mathbf{n}_e\rangle_e \\
&\forall\mathbf{r}_h\in\mathbb{R}_{k-1,*,d}(T),
\end{aligned}
\tag{5.12c}
$$

where $\omega_e:=\frac{1}{2}$ if $e\in\mathcal{E}_h^{\mathrm{int}}$ and $\omega_e:=1$ if $e\in\mathcal{E}_h^{\mathrm{ext}}$

We now check that the above $\mathbf{u}_h$ satisfies Assumption 3.1.

LEMMA 5.4 (Discontinuous Galerkin reconstructed flux property). *Let $\mathbf{u}_h$ be given by Definition 5.3. Then $\mathbf{u}_h$ satisfies Assumption 3.1.*

Proof. Assumption 3.1 (1), i.e., the fact that $\mathbf{u}_h\in\mathbf{V}_h$, is given by the construction (the normal components on sides from $\mathcal{E}_{h,i}^{\mathrm{int}}$ are univalued). Let next $i\in\{1,\dots,n\}$, $T\in\mathcal{T}_{h,i}$, and $\xi_h\in\mathbb{R}_k(T)$ be arbitrary. We then have, using Green's theorem, the fact

that $\xi_h|_e \in \mathbb{R}_k(e)$ for all $e \in \mathcal{E}_T$, $\nabla\xi_h \in \mathbb{R}_{k-1,*,d}(T)$, Definition 5.3 of $\mathbf{u}_h$, and setting $\varphi_h = \xi_h$ on T and $\varphi_h = 0$ otherwise,

$$\begin{aligned}(\nabla{\cdot}\mathbf{u}_h, \xi_h)_T &= -(\mathbf{u}_h, \nabla\xi_h)_T + \sum_{e\in\mathcal{E}_T} \langle \mathbf{u}_h{\cdot}\mathbf{n}_T, \xi_h\rangle_e \\ &= \mathcal{B}_{h,i}(p_h, \lambda_H; \varphi_h) = (f, \varphi_h)_{\Omega_i} = (f, \xi_h)_T.\end{aligned} \tag{5.13}$$

Thus, $\nabla{\cdot}\mathbf{u}_h = \pi_k(f)$, and, consequently Assumption 3.1 (2) follow. Finally, Assumption 3.1 (3) is immediate from (5.10b) noticing that (5.12b) implies, on all $e \in \mathcal{E}_{h,i}^\Gamma$,

$$\mathbf{u}_h|_{\Omega_i}{\cdot}\mathbf{n}_e = -\mathbf{K}\nabla p_h|_{\Omega_i}{\cdot}\mathbf{n}_e + \alpha_g \frac{\sigma_{\mathbf{K},g}}{H_g}\big(p_h|_{\Omega_i} - \pi_{k,\mathcal{E}_{h,i}^\Gamma}(\lambda_H)\big). \qquad \square$$

REMARK 5.5 (Original multiscale mortar discontinuous Galerkin method). *Using in* (5.10b) *directly* λ_H *as proposed in [19] and not* $\pi_{k,\mathcal{E}_{h,i}^\Gamma}(\lambda_H)$, *we can construct* $\mathbf{u}_h|_{\Omega_i}$ *in the higher-order mixed finite element spaces* $\mathbf{RTN}^m(\mathcal{T}_{h,i})$, $i \in \{1,\dots,n\}$, *as in Definition 5.3 (we have to test by* $q_h \in \mathbb{R}_m(e)$ *and* $\mathbf{r}_h \in \mathbb{R}_{m-1,*,d}(T)$. *Assumption 3.1 (2) holds. Note however that neither* $\nabla{\cdot}\mathbf{u}_h = \pi_k(f)$ *nor* $\nabla{\cdot}\mathbf{u}_h = \pi_m(f)$ *holds in this case. Assumption 3.1 (3) is then satisfied by definition from* (5.10b). *Assumption 3.1 (1), however, does not hold true; we have to replace the* k*-th order RTN space* $\mathbf{V}_h$ *by the* m*-th order RTN spaces* $\mathbf{RTN}^m(\mathcal{T}_{h,i})$.

REMARK 5.6 (Lower-order flux recovery in the multiscale mortar discontinuous Galerkin method). *The Definition 5.3 enables to recover the flux from the* k*-th order RTN space* $\mathbf{V}_h$. *Following [22, 15], we can also recover* $\mathbf{u}_h|_{\Omega_i}$ *from* $\mathbf{RTN}^{k-1}(\mathcal{T}_{h,i})$, $i \in \{1,\dots,n\}$, *provided that* $p_h|_{\Omega_i} - \pi_{k,\mathcal{E}_{h,i}^\Gamma}(\lambda_H)$ *and* $p_h|_{\Omega_i} - \lambda_H$ *from* (5.10b) *and* (5.11) *are respectively replaced by* $\pi_{k-1,\mathcal{E}_{h,i}^\Gamma}(p_h|_{\Omega_i} - \lambda_H)$.

REMARK 5.7 (Potential $\tilde{p}_h$ in the multiscale mortar discontinuous Galerkin method). *The solution* $p_h \in W_h$ *can directly be used in Section 3 as* $\tilde{p}_h$, *or a similar postprocessing of* $\tilde{p}_h$ *from* p_h *and* $\mathbf{u}_h$ *as that devised in Section 5.1 can be used. Such potential* $\tilde{p}_h$ *satisfies Assumption 4.1 (1). In any case, however, the multiscale mortar discontinuous Galerkin method, contrarily to the multiscale mortar mixed finite element method of Section 5.1, will not lead to the continuity of* $\tilde{p}_h$ *expressed by Assumptions 4.1 (2)–(3).*

5.3. Multiscale mortar coupled mixed finite element–discontinuous Galerkin method. We give here an example of a multinumerics discretization. Following [19], we consider the multiscale mortar coupled mixed finite element–discontinuous Galerkin method. Let $\mathbf{K}$ be piecewise constant on $\mathcal{T}_h$ in this section once again for simplicity. Let I denote the index set of the subdomains where the k-th order discontinuous Galerkin method is used and J the index set of the subdomains where the k-th order mixed finite element method is used. We then look, for $k \geq 1$, for $p_h|_{\Omega_i} \in W_{h,i}$, $i \in I$, $p_h|_{\Omega_i} \in W_{h,i}$, $i \in J$, $\mathbf{u}_h|_{\Omega_i} \in \mathbf{V}_{h,i}$, $i \in J$, and $\lambda_H \in M_H$ such that

$$\mathcal{B}_{h,i}(p_h, \lambda_H; \varphi_h) = (f, \varphi_h)_{\Omega_i} \quad \forall \varphi_h \in W_{h,i},\ \forall i \in I, \tag{5.14a}$$

$$(\mathbf{K}^{-1}\mathbf{u}_h, \mathbf{v}_h)_{\Omega_i} - (p_h, \nabla{\cdot}\mathbf{v}_h)_{\Omega_i} + \langle \lambda_H, \mathbf{v}_h{\cdot}\mathbf{n}_{\Omega_i}\rangle_{\Gamma_i} = 0 \quad \forall\, \mathbf{v}_h \in \mathbf{V}_{h,i},\ \forall i \in J, \tag{5.14b}$$

$$(\nabla{\cdot}\mathbf{u}_h, w_h)_{\Omega_i} = (f, w_h)_{\Omega_i} \quad \forall w_h \in W_{h,i},\ \forall i \in J, \tag{5.14c}$$

$$\begin{aligned}&\sum_{i\in J} \langle \mathbf{u}_h{\cdot}\mathbf{n}_{\Omega_i}, \mu_H\rangle_{\Gamma_i} + \sum_{i\in I}\sum_{g\in\mathcal{G}_{H,i}} \Big\langle -\mathbf{K}\nabla p_h|_{\Omega_i}{\cdot}\mathbf{n}_{\Omega_i} \\ &\qquad + \alpha_g \frac{\sigma_{\mathbf{K},g}}{H_g}\big(p_h|_{\Omega_i} - \pi_{k,\mathcal{E}_{h,i}^\Gamma}(\lambda_H)\big), \mu_H \Big\rangle_g = 0 \quad \forall \mu_H \in M_H.\end{aligned} \tag{5.14d}$$

The following lemma is a straightforward generalization of the results of the two previous sections:

LEMMA 5.8 (Coupled mixed finite element–discontinuous Galerkin flux property). *Let* $\mathbf{u}_h|_{\Omega_i} \in \mathbf{V}_{h,i}$, $i \in J$, *be given by* (5.14a)–(5.14d). *Define* $\mathbf{u}_h|_{\Omega_i} \in \mathbf{V}_{h,i}$, $i \in I$, *using the flux reconstruction of Definition 5.3. Then* $\mathbf{u}_h$ *satisfies Assumption 3.1.*

5.4. Multiscale mortar finite volume methods. The present approach can be easily extended to finite volume-type multiscale mortar methods and their couplings with other multiscale mortar methods, following the above approach in combination with the results of [31, 17].

6. Proof of the a posteriori estimates. We prove here the a posteriori estimates derived in Section 3.

6.1. Proofs of the a posteriori estimates for the flux. The following theorem follows readily from [33, Theorems 3.1 and 6.1]. Note that it gives an abstract upper bound for the error $|||\mathbf{u}-\mathbf{u}_h|||_*$ which is optimal, up to the factor 2.

THEOREM 6.1 (A general estimate for the flux and its efficiency). *Let* $\mathbf{u}$ *be the exact flux and let* $\mathbf{u}_h \in \mathbf{L}^2(\Omega)$ *be arbitrary. Then*

$$\begin{aligned} |||\mathbf{u}-\mathbf{u}_h|||_* &\le \inf_{s\in H^1_0(\Omega)} |||\mathbf{u}_h+\mathbf{K}\nabla s|||_* + \sup_{\varphi\in H^1_0(\Omega),\,|||\varphi|||=1} \mathcal{A}\left(\mathbf{u}-\mathbf{u}_h,-\mathbf{K}\nabla\varphi\right) \\ &\le 2|||\mathbf{u}-\mathbf{u}_h|||_*. \end{aligned} \tag{6.1}$$

Using this result, we can now justify Theorem 3.2:

Proof. [Proof of Theorem 3.2] The first term in (6.1) clearly leads to the η_{P} estimate of (3.1). Let $\varphi \in H^1_0(\Omega)$ with $|||\varphi||| = 1$ be arbitrary. Using the characterization (2.5) of the weak solution, we have $\mathcal{A}(\mathbf{u},-\mathbf{K}\nabla\varphi) = (f,\varphi)$, whereas

$$\begin{aligned} -\mathcal{A}(\mathbf{u}_h,-\mathbf{K}\nabla\varphi) = (\mathbf{u}_h,\nabla\varphi) &= \sum_{i=1}^n \{-(\nabla\cdot\mathbf{u}_h,\varphi)_{\Omega_i} + \langle \mathbf{u}_h\cdot\mathbf{n}_{\Omega_i},\varphi\rangle_{\partial\Omega_i}\} \\ &= -(\nabla\cdot\mathbf{u}_h,\varphi) + \sum_{i=1}^n \langle \mathbf{u}_h\cdot\mathbf{n}_{\Omega_i},\varphi\rangle_{\partial\Omega_i}, \end{aligned}$$

using Green's theorem. By Assumption 3.1 (2), we have

$$\begin{aligned} (f-\nabla\cdot\mathbf{u}_h,\varphi) &= \sum_{T\in\mathcal{T}_h} (f-\nabla\cdot\mathbf{u}_h,\varphi-\varphi_T)_T \\ &\le \sum_{T\in\mathcal{T}_h} \|f-\nabla\cdot\mathbf{u}_h\|_T\|\varphi-\varphi_T\|_T \le \eta_{\mathrm{R},h}|||\varphi|||, \end{aligned} \tag{6.2}$$

using also Cauchy–Schwarz's inequality, Poincaré's inequality (2.8), and the definition (2.6) of the $|||\cdot|||$ norm. Introduce now a function φ_H, piecewise constant on $\mathcal{G}_H$ and given by $\varphi_g := \langle\varphi,1\rangle_g/|g|$ for all $g\in\mathcal{G}_H$. Note that $\varphi_H \in M_H$ by the assumption on the space M_H. Note also that $\sum_{i=1}^n \langle \mathbf{u}_h\cdot\mathbf{n}_{\Omega_i},\varphi_H\rangle_{\Gamma_i} = 0$ by Assumption 3.1 (3). Using that $\varphi = 0$ on $\partial\Omega_i\cap\partial\Omega$ for all $i\in\{1,\dots,n\}$,

$$\begin{aligned} \sum_{i=1}^n \langle \mathbf{u}_h\cdot\mathbf{n}_{\Omega_i},\varphi\rangle_{\partial\Omega_i} &= \sum_{i=1}^n \langle \mathbf{u}_h\cdot\mathbf{n}_{\Omega_i},\varphi-\varphi_H\rangle_{\Gamma_i} = \tfrac12 \sum_{i=1}^n\sum_{j=1}^n \sum_{g\in\mathcal{G}_{H,i,j}} \langle [\![\mathbf{u}_h\cdot\mathbf{n}_g]\!],\varphi-\varphi_g\rangle_g \\ &\le \tfrac12 \sum_{i=1}^n\sum_{j=1}^n \sum_{g\in\mathcal{G}_{H,i,j}} \|[\![\mathbf{u}_h\cdot\mathbf{n}_g]\!]\|_g C_{\mathrm{t},T_{i,g},g} H_g^{\frac12} c_{\mathbf{K},T_{i,g}}^{-\frac12} |||\varphi|||_{T_{i,g}} \le \eta_{\mathrm{M}}|||\varphi|||. \end{aligned}$$

Here we have used the trace inequality (2.9), the definition (2.6) of the $|||\cdot|||$ norm, and Cauchy–Schwarz's inequality. We have also used the assumption that $T_{i,g}$, $g \in \mathcal{G}_{H,i}$, $i \in \{1,\dots,n\}$, do not overlap. We have expressly carried out the proof with the double sum $\sum_{i=1}^{n}\sum_{j=1}^{n}$, so that the tensor $\mathbf{K}$-dependent constants $c_{\mathbf{K},T_{i,g}}$ are related to the elements $T_{i,g}$ and thus to the individual subdomains Ω_i. The assertion follows by combining the above results. ☐

The following modification of Theorem 6.1 follows easily by adding and subtracting $\mathbf{t} \in \mathbf{H}(\mathrm{div},\Omega)$, by Green's theorem, and by (2.5) as in the proof of Theorem 3.2:

THEOREM 6.2 (A general estimate for the flux and its efficiency). *Let* $\mathbf{u}$ *be the exact flux and let* $\mathbf{u}_h \in \mathbf{L}^2(\Omega)$ *be arbitrary. Then*

$$\begin{aligned}|||\mathbf{u}-\mathbf{u}_h|||_* \le & \inf_{s\in H_0^1(\Omega)} |||\mathbf{u}_h+\mathbf{K}\nabla s|||_* \\ & + \inf_{\mathbf{t}\in\mathbf{H}(\mathrm{div},\Omega)} \left\{ |||\mathbf{u}_h-\mathbf{t}|||_* + \sup_{\varphi\in H_0^1(\Omega),\,|||\varphi|||=1} (f-\nabla\cdot\mathbf{t},\varphi) \right\} \\ & \le 2|||\mathbf{u}-\mathbf{u}_h|||_*.\end{aligned}$$

By virtue of Theorem 6.2, the proof of Theorem 3.3 is immediate, using a similar technique as in (6.2) to treat the term with the source function f.

6.2. Proofs of the a posteriori estimates for the potential. A similar abstract error estimate as that of Theorem 6.1 for the error $|||p-\tilde{p}_h|||$ holds (cf. [30, Lemma 7.1]):

THEOREM 6.3 (A general estimate for the potential and its efficiency). *Let* p *be the exact potential and let* $\tilde{p}_h \in H^1(\mathcal{T}_h)$ *be arbitrary. Then*

$$|||p-\tilde{p}_h||| \le \inf_{s\in H_0^1(\Omega)} |||\tilde{p}_h-s||| + \sup_{\varphi\in H_0^1(\Omega),\,|||\varphi|||=1} \mathcal{A}(\mathbf{K}\nabla(p-\tilde{p}_h),\mathbf{K}\nabla\varphi) \le 2|||p-\tilde{p}_h|||.$$

Using this result, the proof of Theorem 3.4 follows easily by the same arguments as in the proof of Theorem 3.2, noticing that

$$\begin{aligned}\mathcal{A}(\mathbf{K}\nabla(p-\tilde{p}_h),\mathbf{K}\nabla\varphi) &= \mathcal{A}(\mathbf{u}-\mathbf{u}_h,-\mathbf{K}\nabla\varphi) - \mathcal{A}(\mathbf{u}_h+\mathbf{K}\nabla\tilde{p}_h,\mathbf{K}\nabla\varphi) \\ &\le \mathcal{A}(\mathbf{u}-\mathbf{u}_h,-\mathbf{K}\nabla\varphi) + |||\mathbf{u}_h+\mathbf{K}\nabla\tilde{p}_h|||_*\end{aligned}$$

for $\varphi \in H_0^1(\Omega)$ such that $|||\varphi||| = 1$.

The proof of Theorem 3.5 follows from the following consequence of Theorem 6.3:

THEOREM 6.4 (A general estimate for the potential and its efficiency). *Let* p *be the exact potential and let* $\tilde{p}_h \in H^1(\mathcal{T}_h)$ *be arbitrary. Then*

$$\begin{aligned}|||p-\tilde{p}_h||| \le & \inf_{s\in H_0^1(\Omega)} |||\tilde{p}_h-s||| \\ & + \inf_{\mathbf{t}\in\mathbf{H}(\mathrm{div},\Omega)} \sup_{\varphi\in H_0^1(\Omega),\,|||\varphi|||=1} ((f-\nabla\cdot\mathbf{t},\varphi) - (\mathbf{K}\nabla\tilde{p}_h+\mathbf{t},\nabla\varphi)) \\ & \le 2|||p-\tilde{p}_h|||.\end{aligned}$$

7. Proof of the local efficiency. We prove here the local efficiency of our a posteriori estimates announced in Section 4, namely Theorems 4.3–4.5. The proof of Theorem 4.2 is immediate using the triangle inequality.

Proof. [Proof of Theorem 4.3] Let $T' \in \widehat{\mathcal{T}}_h$. Then we proceed as in [31, 33], using the two following fundamental results: Firstly, it follows from [21, 12] that, for any

$\tilde{p}_h \in \mathbb{R}_{r'}(\widehat{\mathcal{T}}_h)$,

$$\|\nabla(\tilde{p}_h - \mathcal{I}_{\mathrm{av}}(\tilde{p}_h))\|_{T'} \leq C \sum_{e' \in \widehat{\mathcal{E}}_h;\, e' \cap T' \neq \emptyset} h_{e'}^{-\frac{1}{2}} \|[\![\tilde{p}_h]\!]\|_{e'}, \tag{7.1}$$

where C depends only on d, r', and $\kappa_{\widehat{\mathcal{T}}_h}$. Secondly, it was established in [2, Theorem 10] that for $e' \in \widehat{\mathcal{E}}_h$ and $\tilde{p}_h \in H^1(\widehat{\mathcal{T}}_h)$ such that $\langle [\![\tilde{p}_h]\!], 1 \rangle_{e'} = 0$,

$$h_{e'}^{-\frac{1}{2}} \|[\![\tilde{p}_h]\!]\|_{e'} \leq C \sum_{T' \in \widehat{\mathcal{T}}_h;\, e' \in \mathcal{E}_{T'}} \|\nabla(\tilde{p}_h - \psi)\|_{T'}, \tag{7.2}$$

where $\psi \in H_0^1(\Omega)$ is arbitrary and C depends only on d and $\kappa_{\widehat{\mathcal{T}}_h}$.

Let $T \in \mathcal{T}_h$ be such that $T \cap \Gamma = \emptyset$. Recall that we have assumed that for $T \in \mathcal{T}_h$ such that $T \cap \Gamma = \emptyset$, there exists an element $T' \in \widehat{\mathcal{T}}_h$ such that $T = T'$. Moreover, every side $e' \in \widehat{\mathcal{E}}_h$ such that $e' \cap T' \neq \emptyset$, again by assumption, either coincides with a side $e \in \mathcal{E}_h^{\mathrm{int}}$ or belongs to the interior of some $T'' \in \mathcal{T}_h$. Recalling the Assumption 4.1 (2), we see that on each such side e', $\langle [\![\tilde{p}_h]\!], 1 \rangle_{e'} = 0$ holds. Combining the above results, we arrive at (setting $\psi = p$)

$$\|\nabla(\tilde{p}_h - \mathcal{I}_{\mathrm{av}}(\tilde{p}_h))\|_T \lesssim \|\nabla(\tilde{p}_h - p)\|_{\mathfrak{T}_T},$$

taking also into account that by assumption, $\widehat{\mathcal{T}}_h$ is a refinement of $\mathcal{T}_h$. Thus, (4.1a) follows after an appropriate scaling with respect to the tensor $\mathbf{K}$.

Let now $T \in \mathcal{T}_h$ such that $T \cap \Gamma \neq \emptyset$ be given. Then

$$\|\nabla(\tilde{p}_h - \mathcal{I}_{\mathrm{av}}(\tilde{p}_h))\|_T^2 = \sum_{T' \in \widehat{\mathcal{T}}_h;\, T' \subset T} \|\nabla(\tilde{p}_h - \mathcal{I}_{\mathrm{av}}(\tilde{p}_h))\|_{T'}^2 \leq C \sum_{e \in \widehat{\mathcal{E}}_h;\, e \cap T \neq \emptyset} h_e^{-1} \|[\![\tilde{p}_h]\!]\|_e^2,$$

using (7.1). For all $e \in \widehat{\mathcal{E}}_h$ such that $e \cap T \neq \emptyset$ and such that $e \not\subset \Gamma$, we have $\langle [\![\tilde{p}_h]\!], 1 \rangle_e = 0$ by the same reasoning as above. Thus we can use directly (7.2). All the other sides e are included in some $g \in \mathcal{G}_h^*$. We now use assumption (2.1). In combination with the assumption that $\widehat{\mathcal{T}}_h$ does not add any nodes on Γ with respect to $\mathcal{T}_h$, we arrive at

$$\sum_{e \in \widehat{\mathcal{E}}_h;\, e \subset g \in \mathcal{G}_h^*,\, g \cap T \neq \emptyset} h_e^{-1} \|[\![\tilde{p}_h]\!]\|_e^2 \leq C_{\mathcal{G}_h^*} \sum_{g \in \mathcal{G}_h^*,\, g \cap T \neq \emptyset} h_g^{-1} \|[\![\tilde{p}_h]\!]\|_g^2.$$

Using now Lemma A.1 instead of (7.2), (4.1b) follows after an appropriate scaling with respect to the tensor $\mathbf{K}$ and setting $\psi = p$. ∎

Proof. [Proof of Theorem 4.4] The assertion of Theorem 4.4 follows immediately using (7.1) and the fact that $\widehat{\mathcal{T}}_h$ is a refinement of $\mathcal{T}_h$. ∎

Proof. [Proof of Theorem 4.5] The proof is decomposed into four parts.

1) Firstly, (4.3a) follows by using the element bubble function technique, cf. [30, Lemma 7.6], whereas (4.3b) is shown as in [35, 6] in combination with (4.3a).

2) We next prove (4.4a)–(4.5b), corresponding to the construction of $\mathbf{t}_h$ from Section 3.3.2.

Let $T \in \mathcal{T}_h \cap \mathcal{T}_H^{\mathrm{int}}$. Then $\eta_{\mathrm{R},H,T}$ coincides with $\eta_{\mathrm{R},h,T}$ and consequently (4.4a) coincides with (4.3a), whereas (4.4b) follows by construction. Let $T \in \mathcal{T}_h$, $T \subset T'$ for some $T' \in \mathcal{T}_H^{\Gamma}$. We then use the estimate

$$\|\mathbf{v}_h\|_{T''}^2 \leq C \left\{ \sum_{e'' \in \mathcal{E}_{T''}} h_{e''} \|\mathbf{v}_h \cdot \mathbf{n}_{e''}\|_{e''}^2 + \left(\sup_{\mathbf{r}_h \in \mathbb{R}_{l-1,*,d}(T'')} \frac{(\mathbf{v}_h, \mathbf{r}_h)_{T''}}{\|\mathbf{r}_h\|_{T''}} \right)^2 \right\},$$

valid for any $T'' \in \widehat{\mathcal{T}}_h$ and any $\mathbf{v}_h \in \mathbf{V}_{\widehat{h}}(T'')$; here $l = k$ or k'. We set $\mathbf{v}_h = \mathbf{u}_h - \mathbf{t}_h$ and use (3.20a)–(3.20b) to infer

$$
\begin{aligned}
|||\mathbf{u}_h - \mathbf{t}_h|||_{*,T} &= \left\{ \sum_{T'' \in \widehat{\mathcal{T}}_h,\, T'' \subset T} |||\mathbf{u}_h - \mathbf{t}_h|||_{*,T''}^2 \right\}^{\frac{1}{2}} \leq C c_{\mathbf{K},T}^{-\frac{1}{2}} \sum_{e \in \mathcal{E}_T} h_e^{\frac{1}{2}} \|[\![\mathbf{u}_h \cdot \mathbf{n}_e]\!]\|_e \\
&\leq C C_{\mathbf{K},\mathfrak{T}_T}^{\frac{1}{2}} c_{\mathbf{K},\mathfrak{T}_T}^{-\frac{1}{2}} |||\mathbf{u} - \mathbf{u}_h|||_{*,\mathfrak{T}_T},
\end{aligned} \tag{7.3}
$$

where for the last estimate, we proceed as in the proof of (4.3b) (note that there is h_e and not H_g in (7.3)). Thus (4.5b) is proved. We are left with bounding $\eta_{\mathrm{R},H,T}$. We have

$$
\eta_{\mathrm{R},H,T} = C_{\mathrm{P},T'} H_{T'} c_{\mathbf{K},T'}^{-\frac{1}{2}} \|f - \nabla \cdot \mathbf{t}_h\|_T \leq C C_{\mathbf{K},T}^{\frac{1}{2}} c_{\mathbf{K},T'}^{-\frac{1}{2}} H_{T'} h_T^{-1} |||\mathbf{u} - \mathbf{t}_h|||_{*,T},
$$

proceeding as in the proof of (4.3a). Combining this with the triangle inequality and (7.3), (4.5a) follows.

3) We now turn to the proof of (4.6)–(4.8), corresponding to the construction of $\mathbf{t}_h$ from Section 3.3.3.

Using the same techniques as before, (4.6) is obvious. Next, the fact that $\tilde{\eta}_{\mathrm{M},T} = 0$ for $T \in \mathcal{T}_h \cap \mathcal{T}_H^{\mathrm{int}}$ is immediate from (3.21). It thus remains to prove (4.8). For $T' \in \mathcal{T}_H^{\Gamma}$, consider $(\mathbf{t}_h', q_h)$ given by the mixed finite element approximation of (3.23a)–(3.23c) on $\widehat{\mathcal{T}}_h|_{T'}$. We will denote by T a generic element of $\widehat{\mathcal{T}}_h|_{T'}$. Considering the postprocessing as in Section 5.1, we obtain $\tilde{q}_h \in \tilde{W}_{\widehat{h}}(T')$ such that $P_{\tilde{\mathbf{V}}_{\widehat{h}}}(-\mathbf{K}\nabla\tilde{q}_h) = \mathbf{t}_h'$ and $P_{W_{\widehat{h}}}(\tilde{q}_h) = q_h$. Here $P_{\tilde{\mathbf{V}}_{\widehat{h}}}$ is the equivalent of $P_{\tilde{\mathbf{V}}_h}$ from Section 5.1 on the mesh $\widehat{\mathcal{T}}_h$ and $P_{W_{\widehat{h}}}$ is given in Section 2.2. Thus

$$
\begin{aligned}
|||\mathbf{t}_h'|||_{*,T'}^2 &= (\mathbf{K}^{-1}\mathbf{t}_h', \mathbf{t}_h')_{T'} = -(\nabla\tilde{q}_h, \mathbf{t}_h')_{T'} = \sum_{T \subset T'} \{(\tilde{q}_h, \nabla\cdot\mathbf{t}_h')_T - \langle \tilde{q}_h, \mathbf{t}_h' \cdot \mathbf{n}_T \rangle_{\partial T}\} \\
&= \langle \tilde{q}_h, \tfrac{1}{2}[\![\mathbf{u}_h \cdot \mathbf{n}_g]\!] \rangle_{\partial T' \cap \Gamma} = \langle \tilde{q}_h - (\tilde{q}_h)_{T'}, \tfrac{1}{2}[\![\mathbf{u}_h \cdot \mathbf{n}_g]\!] \rangle_{\partial T' \cap \Gamma} \\
&\leq C \sum_{g \in \mathcal{G}_H,\, g \subset \partial T'} \|[\![\mathbf{u}_h \cdot \mathbf{n}_g]\!]\|_g H_{T'}^{\frac{1}{2}} c_{\mathbf{K},T'}^{-\frac{1}{2}} |||\tilde{q}_h|||_{T'} \\
&\leq C |||\mathbf{t}_h'|||_{*,T'} \sum_{g \in \mathcal{G}_H,\, g \subset \partial T'} \|[\![\mathbf{u}_h \cdot \mathbf{n}_g]\!]\|_g H_{T'}^{\frac{1}{2}} c_{\mathbf{K},T'}^{-\frac{1}{2}},
\end{aligned}
$$

using Green's theorem, the fact that $\nabla\cdot\mathbf{t}_h' = P_{W_{\widehat{h}}}(f - \nabla\cdot\mathbf{u}_h) = 0$ using the assumption $f - \nabla\cdot\mathbf{u}_h = 0$ made in this case, the fact that $\tilde{q}_h \in \tilde{W}_{\widehat{h}}(T')$ and hence $\langle [\![\tilde{q}_h]\!], \mathbf{t}_h' \cdot \mathbf{n}_e \rangle_e = 0$ for any interior side e of $\widehat{\mathcal{T}}_h|_{T'}$, the fact that $\mathbf{t}_h' \cdot \mathbf{n}_{T'} = 0$ on $\partial T' \setminus \Gamma$ and $\mathbf{t}_h' \cdot \mathbf{n}_{T'} = \frac{1}{2}[\![\mathbf{u}_h \cdot \mathbf{n}_g]\!]$ on all $g \subset \partial T' \cap \Gamma$, the fact that $(\tilde{q}_h, 1)_{T'} = 0$ which follows from the assumption $(q_h, 1)_{T'} = 0$ and from $P_{W_{\widehat{h}}}(\tilde{q}_h) = q_h$, a discrete trace inequality

$$
\|\tilde{q}_h - (\tilde{q}_h)_{T'}\|_g \leq C H_{T'}^{\frac{1}{2}} \|\nabla\tilde{q}_h\|_{T'}
$$

which can be obtained as discrete Poincaré's and Friedrichs' inequalities in [29, Theorems 5.4 and 8.1], and finally the inequality (cf. [33, Lemma 5.4]) $|||\tilde{q}_h|||_{T'} \leq C|||\mathbf{t}_h'|||_{*,T'}$. The proof is finished recalling that $\mathbf{t}_h' = \mathbf{t}_h - \mathbf{u}_h$ and using (4.3b).

4) We finally prove (4.9a)–(4.9b), corresponding to the construction of $\mathbf{t}_h$ from Section 3.3.4.

Firstly, we show (4.9a). Let $T' \in \mathcal{T}_H$ be given. Then, using the element bubble function technique as in the step 1) and the triangle inequality,

$$C_{\mathrm{P},T'} H_{T'} c_{\mathbf{K},T'}^{-\frac{1}{2}} \|f - \nabla\cdot\mathbf{t}_h\|_{T'} \leq C C_{\mathbf{K},T'}^{\frac{1}{2}} c_{\mathbf{K},T'}^{-\frac{1}{2}} (|||\mathbf{u}_h - \mathbf{t}_h|||_{*,T'} + |||\mathbf{u} - \mathbf{u}_h|||_{*,T'}).$$

Secondly, for a fixed $i \in \{1,\ldots,n\}$, consider the following subdomain problem:

$$-\nabla\cdot(\mathbf{K}\nabla q) = f \qquad \text{in } \Omega_i, \tag{7.4a}$$

$$-\mathbf{K}\nabla q\cdot\mathbf{n}_{\Omega_i} = F(\mathbf{n}_{\Omega_i}\cdot\mathbf{n}_\Gamma) \qquad \text{on } \partial\Omega_i, \tag{7.4b}$$

$$(q,1)_{\Omega,i} = (p,1)_{\Omega,i}. \tag{7.4c}$$

Denote by $(\mathbf{t}_H^\#, q_H^\#)$ its mixed finite element approximation in $\mathbf{V}_{H,F,\Omega_i} \times W_H(\Omega_i)$ (recall that this space was defined in Section 3.3.4). This approximation is not to be computed, it is only introduced for the analysis. We then have

$$|||\mathbf{u}_h - \mathbf{t}_h|||_{*,\Omega_i} \leq |||\mathbf{u}_h - \mathbf{t}_H^\#|||_{*,\Omega_i} \leq |||\mathbf{t}_H^\# + \mathbf{K}\nabla q|||_{*,\Omega_i} + |||\mathbf{u}_h + \mathbf{K}\nabla q|||_{*,\Omega_i},$$

using (3.25) and the triangle inequality. Supposing that q is smooth enough, we have

$$|||\mathbf{t}_H^\# + \mathbf{K}\nabla q|||_{*,\Omega_i} \leq C H^{m+1}. \tag{7.5}$$

Using [33, Theorem 3.1], we have

$$|||\mathbf{u}_h + \mathbf{K}\nabla q|||_{*,\Omega_i} \leq |||\mathbf{u}_h + \mathbf{K}\nabla p|||_{*,\Omega_i} + \left| \left(\mathbf{u}_h + \mathbf{K}\nabla q, \frac{\nabla(p-q)}{|||p-q|||_{\Omega_i}} \right)_{\Omega_i} \right|.$$

Set $\varphi := (p-q)/|||p-q|||_{\Omega_i}$ and note that $\varphi \in H^1(\Omega_i)$, $\varphi_{\Omega_i} = 0$. Thus

$$\begin{aligned}
&|||\mathbf{u}_h + \mathbf{K}\nabla q|||_{*,\Omega_i} \\
&\leq |||\mathbf{u}_h - \mathbf{u}|||_{*,\Omega_i} + |(\mathbf{u}_h + \mathbf{K}\nabla q, \nabla\varphi)_{\Omega_i}| \\
&= |||\mathbf{u}_h - \mathbf{u}|||_{*,\Omega_i} + |(f - \nabla\cdot\mathbf{u}_h, \varphi)_{\Omega_i} + \langle (\mathbf{u}_h + \mathbf{K}\nabla q)\cdot\mathbf{n}_{\Omega_i}, \varphi\rangle_{\partial\Omega_i}| \\
&= |||\mathbf{u}_h - \mathbf{u}|||_{*,\Omega_i} + |(f - \nabla\cdot\mathbf{u}_h, \varphi)_{\Omega_i} + \langle \mathbf{u}_h\cdot\mathbf{n}_{\Omega_i} - F(\mathbf{n}_{\Omega_i}\cdot\mathbf{n}_\Gamma), \varphi - P_{M_H}(\varphi)\rangle_{\partial\Omega_i}| \\
&\leq |||\mathbf{u}_h - \mathbf{u}|||_{*,\Omega_i} + \eta_{\mathrm{R},h,\Omega_i} + \|\mathbf{u}_h\cdot\mathbf{n}_{\Omega_i} - F(\mathbf{n}_{\Omega_i}\cdot\mathbf{n}_\Gamma)\|_{\partial\Omega_i} \|\varphi - P_{M_H}(\varphi)\|_{\partial\Omega_i}.
\end{aligned}$$

The first term in the above expression is directly the actual error, the second one is of higher order/can be bounded by (4.3a), and if both p and q (and consequently φ) are smooth enough, [6, estimate (3.5)] gives

$$\|\varphi - P_{M_H}(\varphi)\|_{\partial\Omega_i} \leq C H^{m+1}. \tag{7.6}$$

Both estimates (7.5) and (7.6) are, of course, imperfect as C is unknown and depends on the smoothness of p and q; moreover, there is the additional quantity $\|\mathbf{u}_h\cdot\mathbf{n}_{\Omega_i} - F(\mathbf{n}_{\Omega_i}\cdot\mathbf{n}_\Gamma)\|_{\partial\Omega_i}$, which is, however, expected to be bounded in view of (3.18). ∎

8. Numerical experiments. We present here several numerical experiments illustrating the a posteriori error estimates for different numerical methods.

The $H_0^1(\Omega)$-conforming potential reconstruction s_h will always be constructed following Section 3.3.1. The different a posteriori error estimators corresponding to the four cases of Theorem 4.5 will be given the following shorthand notations:

- Method 1: The a posteriori error estimates are given by Theorems 3.2 and 3.4. In particular, the notion of the $\mathbf{H}(\mathrm{div},\Omega)$-conforming flux reconstruction $\mathbf{t}_h$ is not needed here.

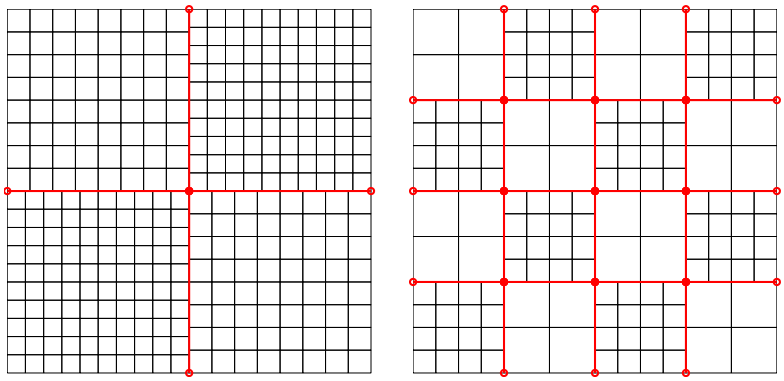

FIG. 8.1. *Initial subdomains grid $\mathcal{T}_h$ and interface grid $\mathcal{G}_H$, Section 8.1 (left) and Section 8.2 (right)*

- Method 2: The a posteriori error estimates are given by Theorems 3.3 and 3.5. The $\mathbf{H}(\mathrm{div},\Omega)$-conforming flux reconstruction $\mathbf{t}_h$ is constructed by direct prescription of Section 3.3.2.
- Method 3: The a posteriori error estimates are given by Theorems 3.3 and 3.5. The $\mathbf{H}(\mathrm{div},\Omega)$-conforming flux reconstruction $\mathbf{t}_h$ is constructed by solving h-grid-size k-th order local Neumann problems of Section 3.3.3.
- Method 4: The a posteriori error estimates are given by Theorems 3.3 and 3.5. The $\mathbf{H}(\mathrm{div},\Omega)$-conforming flux reconstruction $\mathbf{t}_h$ is constructed by solving H-grid-size m-th order local Neumann problems of Section 3.3.4.

The paper focuses on three major issues: mortars, multiscale, and multinumerics; so we consider three test examples, each emphasizing one of the issues. We always reduce the problem to a coarse scale interface operator and use the multiscale mortar basis method developed in [18, 34] to solve the coarse scale interface equation.

8.1. Mortar coupling. This first example focuses on the mortar coupling. We solve on $\Omega := (0,1)\times(0,1)$ the problem (1.1a)–(1.1b) with a diagonal highly oscillating tensor coefficient $\mathbf{K}$,

$$\mathbf{K} := \begin{cases} 15 - 10\sin(10\pi x)\sin(10\pi y), & x,y \in (0,1/2) \text{ or } x,y \in (1/2,1), \\ 15 - \sin(2\pi x)\sin(2\pi y), & \text{otherwise.} \end{cases}$$

We impose the source term f according to the analytic solution

$$p(x,y) = x(1-x)y(1-y).$$

We use the multiscale mortar mixed finite element method (5.1a)–(5.1c). The domain Ω is divided into four subdomains Ω_i with the interface Γ along the lines $x = 1/2$ and $y = 1/2$. In each subdomain Ω_i, we use the lowest-order Raviart–Thomas–Nédélec mixed finite element method on a square mesh $\mathcal{T}_{h,i}$, $\mathbf{V}_{h,i} := \mathbf{RTN}^0(\mathcal{T}_{h,i})$, $W_{h,i} := \mathbb{R}_0(\mathcal{T}_{h,i})$. Thus $k = 0$. The mortar space M_H is the space of discontinuous first-order polynomials on the interface mesh $\mathcal{G}_H$. Thus $m = 1$. The meshes $\mathcal{T}_{h,i}$ do not match along the interface Γ. For initial meshes $\mathcal{T}_{h,i}$, we use 8×8 and 10×10 square grids alternated in a checkerboard fashion (so, initially, $h = \sqrt{2}/16$). The initial mortar grid $\mathcal{G}_H$ has one element on all $\mathcal{G}_{H,i,j}$, so that $H = 1/2$ for the coarsest mesh. We refer to Figure 8.1 (left) for the visualization of this setting. We run several

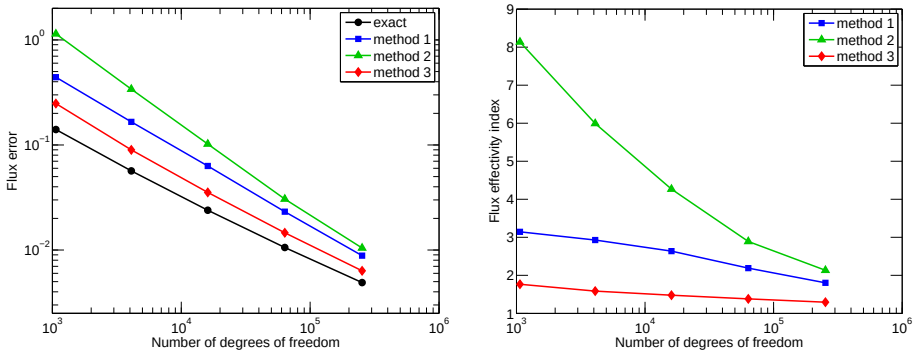

FIG. 8.2. *Estimated and actual flux error (left) and effectivity indices (right) on uniformly refined meshes using methods 1, 2, and 3 for Section 8.1*

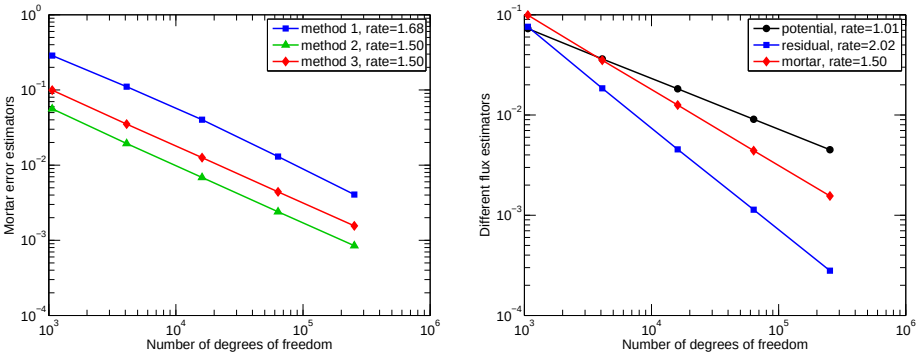

FIG. 8.3. *Mortar estimators using methods 1, 2, and 3 (left) and different estimators using method 3 (right) on uniformly refined meshes for Section 8.1*

levels of uniform grid refinement where we always halve both subdomain and mortar element diameters, so that $H = 4\sqrt{2}h$ on each level. Note that this setting is rather extreme, with coarse mortar grid and fine subdomain grids and relatively increased $C_{\mathcal{G}_h^*} = 5$. We have chosen it purposely so that the mortar error is significant.

Figure 8.2 (left) compares the actual and estimated flux errors $|||\mathbf{u}-\mathbf{u}_h|||_*$ against the total number of degrees of freedom for the methods 1, 2, and 3. Firstly, we see that in all of the cases, the estimates give an upper bound on the error, as predicted by the theory. The corresponding effectivity indices, given as the ratios of the estimate over the error, are plotted in Figure 8.2 (right). We give some more details in Figure 8.3 (left), where we plot the mortar estimator η_{M} for method 1 and the mortar estimators $\tilde{\eta}_{\mathrm{M}}$ for methods 2 and 3. As predicted by the theory, see the discussion following Theorem 3.2, the mortar error is overestimated in method 1. Its convergence rate is roughly the same as for the estimators $\tilde{\eta}_{\mathrm{M}}$, but the actual value of the estimate is increased. Methods 2 and 3 show better results for the mortar error only. In method 2, however, a part of the actual mortar error is also estimated by the residual estimator $\eta_{\mathrm{R},H}$ of (3.6) which does not correspond to data oscillation (and is not as efficient as the other estimators, see (4.5a)). In method 3, on the contrary, $\eta_{\mathrm{R},H}$ of (3.6) takes the superconvergent form of $\eta_{\mathrm{R},\widehat{h}}$ given by (3.13), see Remark 3.6. Thus, finally, method 3 gives the best results, followed by methods 1 and 2, as Figure 8.2 demonstrates.

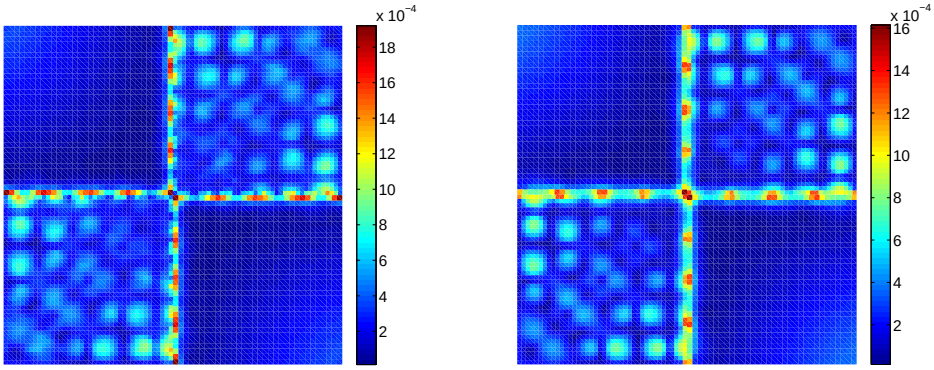

FIG. 8.4. *Estimated (left) and actual (right) flux error distribution on a uniformly refined mesh using method 3 for Section 8.1*

Figure 8.3 (right) compares the flux estimators η_{P}, $\eta_{\mathrm{R},H} = \eta_{\mathrm{R},\widehat{h}}$, and $\tilde{\eta}_{\mathrm{M}}$ for method 3. The estimator η_{P}, the same as the flux error $|||\mathbf{u} - \mathbf{u}_h|||_*$, converges as $\mathcal{O}(h)$. Since f is smooth, $\eta_{\mathrm{R},H} = \eta_{\mathrm{R},\widehat{h}}$ converges as $\mathcal{O}(h^2)$. It is interesting to notice that $\tilde{\eta}_{\mathrm{M}}$ converges here faster than $\mathcal{O}(h)$ and eventually gets negligible. For the same reason, all methods 1, 2, and 3 approach mutually in the overall precision with increasing refinement level, cf. Figure 8.2.

We next show in Figure 8.4 the estimated and actual spatial distribution of the flux errors $|||\mathbf{u} - \mathbf{u}_h|||_*$ of method 3 on the third level refinement. We can see that the error estimator can detect the actual error distribution (and not only its size, like indicated by the effectivity indices given in Figure 8.2 (right)) very well. In particular, both the error inside each subdomain and the mortar error along the interface Γ are well predicted. The distribution of the predicted mortar error $\tilde{\eta}_{\mathrm{M}}$ of method 3 itself corresponds to the increased values along the lines $x = 1/2$ and $y = 1/2$ in Figure 8.4. Note that $\tilde{\eta}_{\mathrm{M}}$ in method 3 is a volumetric quantity and can be nonzero in a band of width H around the interface Γ, see Section 3.3.3. Once again, we have purposely used quite coarse mortar mesh, so as to obtain rather increased mortar error.

8.2. Multiscale. The second example focuses on the multiscale setting and compares methods 1, 3, and 4. We solve on $\Omega := (0,1) \times (0,1)$ the problem (1.1a)–(1.1b) with a full tensor coefficient $\mathbf{K}$,

$$\mathbf{K} := \begin{pmatrix} 3 & 2 \\ 2 & 3 \end{pmatrix},$$

and we impose the source term f according to the analytic solution

$$p(x,y) = \sin(2\pi x)\sin(2\pi y).$$

Note that such a solution belongs to $C^\infty(\Omega)$ and hence is smooth enough for the proof of Theorem 4.5, part 4).

As in the previous example, we use the multiscale mortar mixed finite element method (5.1a)–(5.1c). The subdomains Ω_i, the initial subdomain meshes $\mathcal{T}_{h,i}$, and the mortar mesh $\mathcal{G}_H$ are illustrated in Figure 8.1 (right). We keep $\mathbf{V}_{h,i} := \mathbf{RTN}^0(\mathcal{T}_{h,i})$, $W_{h,i} := \mathbb{R}_0(\mathcal{T}_{h,i})$, i.e., $k = 0$. We, however, increase the polynomial order approximation on the interface mesh $\mathcal{G}_H$. More precisely, we consider two cases, where M_H

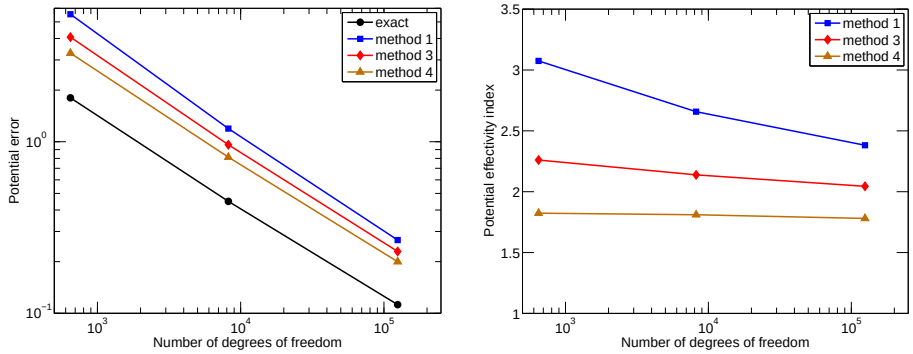

FIG. 8.5. *Estimated and actual potential error (left) and effectivity indices (right) on uniformly refined meshes using methods 1, 3, and 4 for Section 8.2, case (a)*

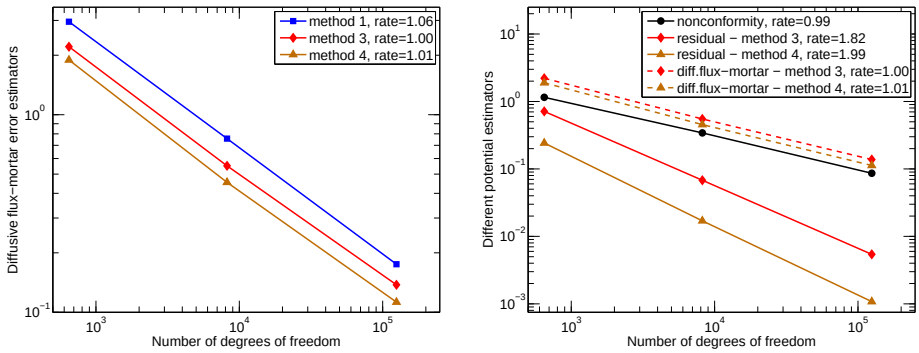

FIG. 8.6. *Diffusive flux–mortar estimators using methods 1, 3, and 4 (left) and different potential estimators using methods 3 and 4 (right) on uniformly refined meshes for Section 8.2, case (a)*

consists of discontinuous piecewise quadratic polynomials, i.e., $m = 2$, in case (a), and of discontinuous piecewise linear polynomials, i.e., $m = 1$, in case (b). For both cases, we run several levels of uniform grid refinement where we halve mortar element diameters and reduce four times the subdomain element diameters, so $H = 2^{-\frac{3}{4}}\sqrt{h}$ on each level.

Case (a) corresponds to the a priori analysis of [6]. The present experiments indicate that case (b) is also computationally possible. This case is much more computationally efficient (recall that (5.1a)–(5.1c) can be reduced to an interface problem on M_H, which is given in case (b) by piecewise first-order polynomials on $\mathcal{G}_H$ only) and it appears here that it has the same accuracy (the overall error still decreases as $\mathcal{O}(h)$). The present a posteriori estimates can be used to monitor and verify this asymptotic accuracy. Note also that in case (b), the mortar error is expected to be rather significant and presents a challenging test case for the robustness of the mortar estimators.

Figures 8.5 and 8.6 show the results for case (a) and Figures 8.7 and 8.8 for case (b). As predicted by Theorem 4.5, the estimator η_{M} of method 1 and $\tilde{\eta}_{\mathrm{M}}$ of method 3 are not robust with respect to the ratio H/h (see Figure 8.8, where these estimators clearly decay with a slope inferior to $\mathcal{O}(h)$ of $\eta_{\mathrm{P},T}$ and of $|||\mathbf{u}-\mathbf{u}_h|||_*$). Consequently, the effectivity index for method 1 (see Figure 8.7 (right)), although quite

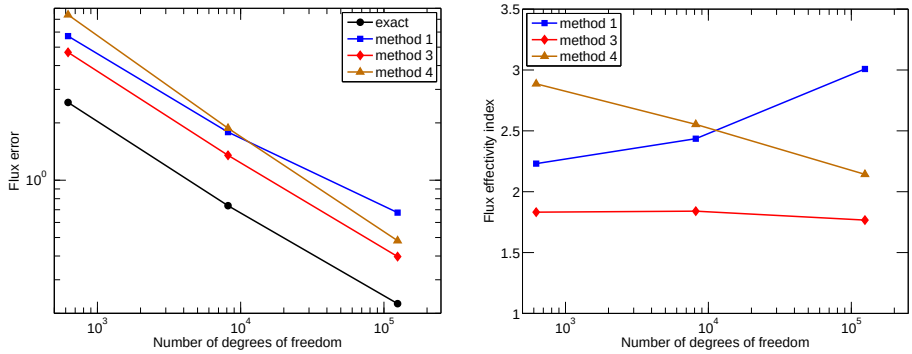

FIG. 8.7. *Estimated and actual flux error (left) and effectivity indices (right) on uniformly refined meshes using methods 1, 3, and 4 for Section 8.2, case (b)*

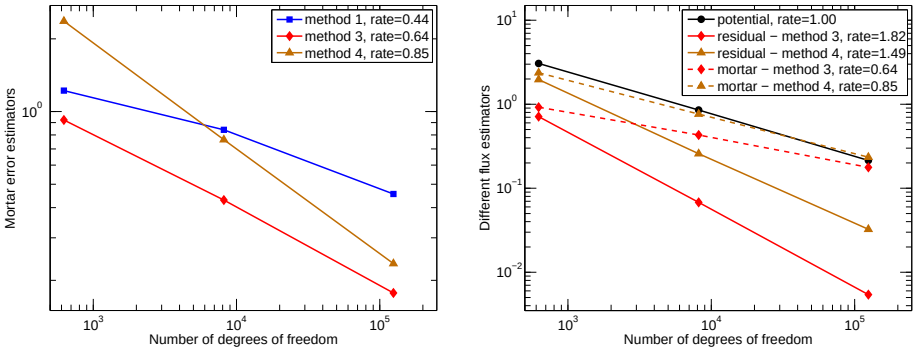

FIG. 8.8. *Mortar estimators using methods 1, 3, and 4 (left) and different flux estimators using methods 3 and 4 (right) on uniformly refined meshes for Section 8.2, case (b)*

close to the optimal value of one on coarse meshes, grows with the refinement level. On the other hand, as predicted by Theorem 4.5 in conjunction with Remark 4.9, the estimator $\tilde{\eta}_{\mathrm{M}}$ of method 4 is fully robust with respect to the ratio H/h (see Figure 8.6, where $\tilde{\eta}_{\mathrm{M}}$ for method 4 decays with the slope $\mathcal{O}(h)$ of $\eta_{\mathrm{P},T}$ and of $|||\mathbf{u}-\mathbf{u}_h|||_*$). Consequently, for method 4, the effectivity index is not increasing but rather decreasing with the refinement level. The rate in Figure 8.8 is no longer optimal (0.85 instead of 1), but still much better than 0.64 of method 3. Recall that case (b) is not covered by the theory of [6], so that the robustness conclusions of Theorem 4.5 and Remark 4.9 do not apply to it. The estimated and the actual spatial distribution of the flux errors $|||\mathbf{u}-\mathbf{u}_h|||_*$ in case (a) for method 4 on the third level of refinement are shown in Figure 8.9. Once again, they match very well. Recall that the mortar estimator $\tilde{\eta}_{\mathrm{M}}$ is by construction nonzero in the entire domain, as we, by the problems (3.24a)–(3.24b), redistribute the mortar mass balance interface error over the entire subdomains Ω_i.

8.3. Multinumerics and adaptivity. The third example focuses on the multinumerics and local adaptivity of both the subdomain and mortar grids. We solve on $\Omega := (-1,1)\times(-1,1)$ the problem (1.1a)–(1.1b) with a piecewise constant $\mathbf{K}$,

$$\mathbf{K} := \begin{cases} 5 & (x,y) \in (-1,0)\times(-1,0) \text{ or } (x,y)\in(0,1)\times(0,1), \\ 1 & \text{otherwise.} \end{cases}$$

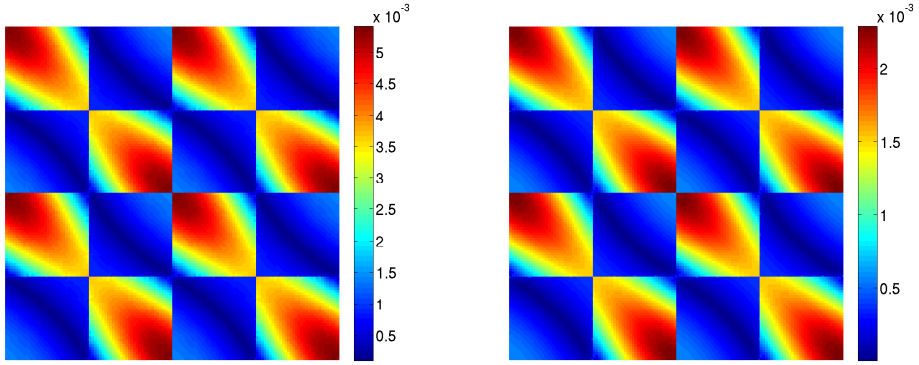

FIG. 8.9. *Estimated (left) and actual (right) flux error distribution on a uniformly refined mesh using method 4 for Section 8.2, case (a)*

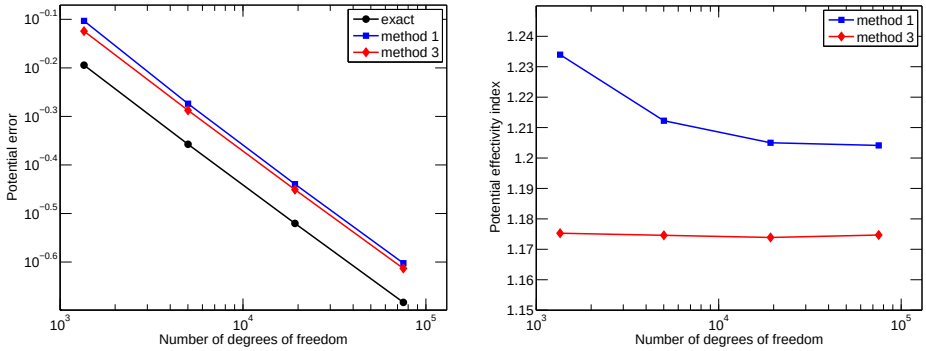

FIG. 8.10. *Estimated and actual potential error (left) and effectivity indices (right) on uniformly refined meshes using methods 1 and 3 for Section 8.3*

We impose the source term f and Dirichlet boundary conditions according to the analytic solution, which is given by (in polar coordinates)

$$p(r,\theta)|_i = r^\alpha(a_i \sin(\alpha\theta) + b_i \cos(\alpha\theta)),$$

where $i \in \{1,\dots,4\}$ corresponds to the axis quadrants and where $\alpha = 0.53544$, $a_1 = 0.44721$, $b_1 = 1$, $a_2 = -0.74536$, $b_2 = 2.33333$, $a_3 = -0.94412$, $b_3 = 0.55556$, $a_4 = -2.4017$, and $b_4 = -0.48148$. Inhomogeneous Dirichlet boundary conditions are set according the solution; the error stemming from their discrete approximation is neglected. This solution has been studied previously in [27, 30, 31] and provides an excellent test for a posteriori error estimation and adaptive mesh refinement due to the singularity at the point $(0,0)$.

The domain Ω is divided into sixteen subdomains Ω_i with the interface Γ along the lines $x = -1/2, 0, 1/2$ and $y = -1/2, 0, 1/2$. On the inner subdomains, i.e., those which intersect the point $(0,0)$ where the singularity resides, we use piecewise linear NIP discontinuous Galerkin finite element method on triangular meshes. In the remaining subdomains we use the lowest-order Raviart–Thomas–Nédélec mixed finite element method on a square mesh. The coupling is achieved via (5.14a)–(5.14d).

The mortar space M_H is the space of discontinuous second-order polynomials on the interface mesh $\mathcal{G}_H$ ($m = 2$). For initial meshes we use 4×4 rectangular meshes

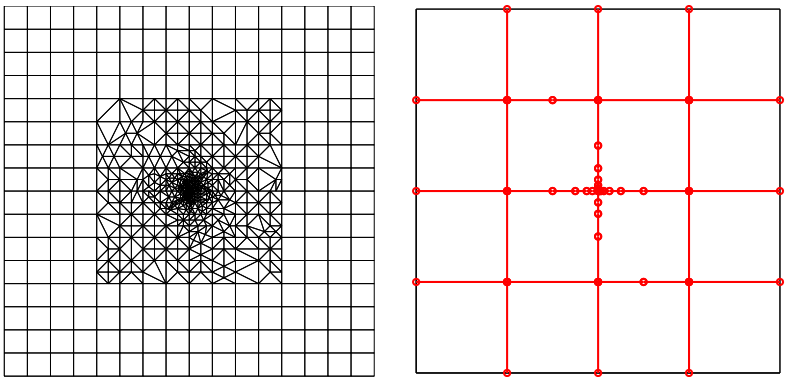

FIG. 8.11. *Adaptive subdomain mesh (left) and mortar mesh (right) after 12 steps of adaptive refinement for Section 8.3*

in the mixed subdomains and the same 4×4 meshes divided into triangles in the discontinuous Galerkin subdomains. The initial mortar grid $\mathcal{G}_H$ has one element on all $\mathcal{G}_{H,i,j}$, so that $H = 1/4$ for the coarsest mesh. We note that the initial subdomain grids match along the interface, but as we have seen in the previous examples, this is not required and in the adaptive algorithm the subdomains may each be refined independently.

Figure 8.10 (left) compares the actual and estimated potential errors for the methods 1 and 3 on uniformly refined meshes. The estimates give an upper bound on the error, as predicted by the theory. The corresponding effectivity indices are plotted in Figure 8.10 (right). We see that they remain relatively constant as the grids are refined.

Next, we use the a posteriori error estimate for adaptive mesh refinement. For our refinement criteria, we compute the maximum of the subdomain and mortar error indicators and mark a subdomain or mortar mesh for refinement if its error indicator is larger that 0.8 times this maximum. Within the mixed subdomains the grids are refined uniformly, while within the discontinuous Galerkin subdomains and the mortars the elements are refined independently. The numerical simulator we use requires conforming meshes within each subdomain, so we remove any hanging nodes by refining neighboring elements, although in general this is not necessary for discontinuous Galerkin.

Figure 8.11 shows the adapted subdomain mesh (left) and the adapted mortar mesh (right) after twelve levels of refinement using method 3. We see that the adaptivity is concentrated around the singularity as one might expect. Figure 8.12 (left) compares the actual and estimated flux errors $|||\mathbf{u} - \mathbf{u}_h|||_*$ and potential errors $|||p - \tilde{p}_h|||_*$ using method 3 on adaptively refined meshes. The corresponding effectivity indices are plotted in Figure 8.12 (right). We see that method 3 accurately predicts the decay in both errors as the mesh is refined.

Finally, in Figure 8.13 we compare the estimated and actual flux errors (left) and potential errors (right) on uniform and adaptive meshes. Clearly, the adaptively refined meshes are able to provide an accurate solution with far fewer degrees of freedom. The convergence order is approximately $\mathcal{O}(h^{0.55})$ for uniform refinement and $\mathcal{O}(h^{1.03})$ for the adaptive algorithm which indicates that the refinement resolves the singularity.

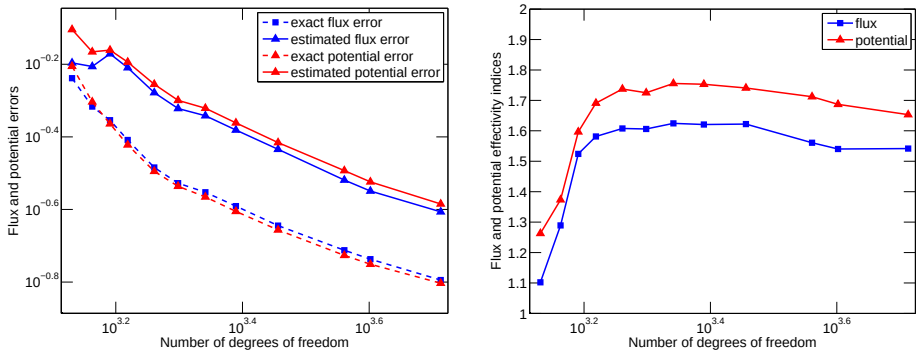

FIG. 8.12. *Estimated and actual flux error and potential error (left) and effectivity indices (right) on adaptively refined meshes using method 3 for Section 8.3*

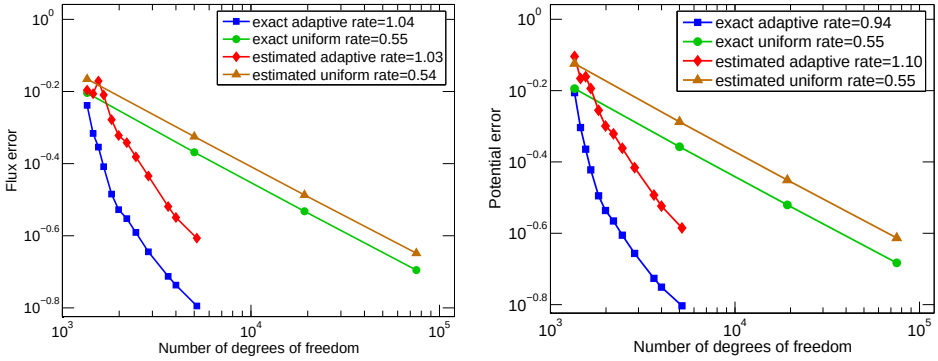

FIG. 8.13. *Estimated and actual flux error (left) and potential error (right) on uniformly and adaptively refined meshes using method 3 for Section 8.3*

9. Concluding remarks. We have introduced here a general framework for guaranteed a posteriori error estimates for multiscale, multinumerics, and mortar coupling. In Sections 4 and 8, we have classified the various estimators of Section 3 into four methods. Method 1, where the estimates are given by Theorems 3.2 and 3.4 and where no notion of the $\mathbf{H}(\mathrm{div},\Omega)$-conforming flux reconstruction $\mathbf{t}_h$ appears, is the easiest to implement and the cheapest to evaluate. It gives quite good results. Method 3, where the estimates are given by Theorems 3.3 and 3.5 and the $\mathbf{H}(\mathrm{div},\Omega)$-conforming flux reconstruction $\mathbf{t}_h$ following Section 3.3.3, is slightly more involved to implement and requires the solution of local Neumann problems. It, however, gives the best results for almost all the test cases. Method 2, with $\mathbf{t}_h$ constructed following Section 3.3.2, is cheaper than method 3 but gives worse results and should be avoided. Method 4, with $\mathbf{t}_h$ constructed following Section 3.3.4, is the most expensive but the only one robust in the multiscale setting of the multiscale mortar mixed finite element method, under sufficient regularity assumptions.

Appendix A. A technical result. We give here a technical result which was necessary in the proof of Theorem 4.3 in Section 7.

LEMMA A.1. *Let $\tilde{p}_h \in H^1(\mathcal{T}_h)$ satisfying Assumptions 4.1 (2)–(3) be given. Then*

$$h_g^{-\frac{1}{2}} \|[\![\tilde{p}_h]\!]\|_g \leq C \sum_{T\in\mathcal{T}_h;\, |g\cap\partial T|\neq 0} \|\nabla(\tilde{p}_h - \psi)\|_T$$

for all $g \in \mathcal{G}_h^*$, where $\psi \in H^1(\Omega)$ is arbitrary and C depends on d, $\kappa_{\mathcal{T}_h}$, and $C_{\mathcal{G}_h^*}$.

Proof. The proof is a generalization of [2, Theorem 10] to the case where $g \in \mathcal{G}_h^*$ is, from each side of the interface, a union of sides from $\mathcal{E}_h^\Gamma$, not necessarily matching, such that only $\langle [\![\tilde{p}_h]\!], 1\rangle_g = 0$ holds. If not specified otherwise, C denotes a generic constant depending on d, $\kappa_{\mathcal{T}_h}$, and $C_{\mathcal{G}_h^*}$, not necessarily the same at each occurrence.

Consider $g \in \mathcal{G}_h^*$ and all the elements T_i' and T_j'' of $\mathcal{T}_h$ from the two subdomains Ω_i and Ω_j such that $|g\cap\partial T_i'| \neq 0$ and $|g\cap\partial T_j''| \neq 0$, cf. Figure 2.1. Denote $\cup T_i'$ by T' and $\cup T_j''$ by T''. Note that T' and T'' are not elements of $\mathcal{T}_h$ but unions of elements of $\mathcal{T}_h$. We will herein use the letter T to denote an element of $\mathcal{T}_h$. In each of T' and T'', $T^* = T', T''$, consider the following Neumann problem:

$$-\Delta\varphi = 0 \qquad \text{in } T^*, \tag{A.1a}$$

$$\nabla\varphi\cdot\mathbf{n}_g = [\![\tilde{p}_h]\!] \quad \text{on } \partial T^* \cap g, \tag{A.1b}$$

$$\nabla\varphi\cdot\mathbf{n}_{T^*} = 0 \qquad \text{on } \partial T^* \setminus g, \tag{A.1c}$$

$$(\varphi, 1)_{T^*} = 0. \tag{A.1d}$$

Note that these problems are well-posed, using Assumption 4.1 (3). Let now $\psi \in H^1(T'\cup T'')$ be arbitrary. Set $\tilde{\psi}|_{T'} := \psi|_{T'} + c_{T'}$ and $\tilde{\psi}|_{T''} := \psi|_{T''} + c_{T''}$, where $c_{T'} := (\tilde{p}_h - \psi)_{T'}$ and $c_{T''} := (\tilde{p}_h - \psi)_{T''}$. The function ψ is on T', T'' shifted by the constants $c_{T'}$ and $c_{T''}$ so that $\tilde{\psi}$ has a the same mean value as $\tilde{p}_h$ on both T', T'',

$$(\tilde{\psi}, 1)_{T'} = (\tilde{p}_h, 1)_{T'}, \tag{A.2a}$$

$$(\tilde{\psi}, 1)_{T''} = (\tilde{p}_h, 1)_{T''}. \tag{A.2b}$$

Now develop

$$\begin{aligned}(\nabla\varphi, \nabla(\tilde{\psi} - \tilde{p}_h))_{T'\cup T''} &= \sum_{T\subset T'\cup T''} (\nabla\varphi, \nabla(\tilde{\psi} - \tilde{p}_h))_T = \sum_{T\subset T'\cup T''} \langle \nabla\varphi\cdot\mathbf{n}_T, \tilde{\psi} - \tilde{p}_h\rangle_{\partial T} \\ &= -\|[\![\tilde{p}_h]\!]\|_g^2 + \langle [\![\tilde{p}_h]\!], [\![\tilde{\psi}]\!]\rangle_g + \sum_{T\subset T'\cup T''} \langle \nabla\varphi\cdot\mathbf{n}_T, \tilde{\psi} - \tilde{p}_h\rangle_{\partial T} \\ &\quad - \sum_{T\subset T'\cup T''} \mathbf{n}_T\cdot\mathbf{n}_g \langle [\![\tilde{p}_h]\!], \tilde{\psi} - \tilde{p}_h\rangle_{\partial T\cap g},\end{aligned}$$

using Green's theorem (note that $\tilde{p}_h$ is by assumption only regular on the elements T of $\mathcal{T}_h$) and (A.1a). This leads to

$$\begin{aligned}\|[\![\tilde{p}_h]\!]\|_g^2 \leq{}& \|\nabla\varphi\|_{T'\cup T''} \|\nabla(\tilde{\psi} - \tilde{p}_h)\|_{T'\cup T''} + \sum_{T\subset T'\cup T''} \|\nabla\varphi\cdot\mathbf{n}_T\|_{-\frac{1}{2},\partial T} \|\tilde{\psi} - \tilde{p}_h\|_{\frac{1}{2},\partial T} \\ &+ \sum_{T\subset T'\cup T''} \|[\![\tilde{p}_h]\!]\|_{\partial T\cap g} \|\tilde{\psi} - \tilde{p}_h\|_{\partial T\cap g} + |\langle [\![\tilde{p}_h]\!], [\![\tilde{\psi}]\!]\rangle_g|.\end{aligned} \tag{A.3}$$

(Here we use the definitions $\|\cdot\|_{-\frac{1}{2},\partial T}$ and $\|\cdot\|_{\frac{1}{2},\partial T}$ as in [24].) We now estimate each of the above right-hand-side terms separately.

1) First of all,

$$\|\nabla\varphi\|_{T'}^2 = \langle \nabla\varphi\cdot\mathbf{n}_{T'}, \varphi\rangle_{\partial T'} = \mathbf{n}_{T'}\cdot\mathbf{n}_g\langle [\![\tilde{p}_h]\!], \varphi\rangle_g \le C\|[\![\tilde{p}_h]\!]\|_g h_g^{\frac{1}{2}}\|\nabla\varphi\|_{T'},$$

where C is the constant from the trace inequality

$$\|\varphi\|_g \le C h_g^{\frac{1}{2}}\|\nabla\varphi\|_{T'}$$

(recall that (A.1d) holds). As a similar estimate on T'' can be established likewise, it follows that the first term of (A.3) can be bounded by

$$C\|[\![\tilde{p}_h]\!]\|_g h_g^{\frac{1}{2}}\|\nabla(\tilde{\psi}-\tilde{p}_h)\|_{T'\cup T''} = C\|[\![\tilde{p}_h]\!]\|_g h_g^{\frac{1}{2}}\|\nabla(\psi-\tilde{p}_h)\|_{T'\cup T''}. \tag{A.4}$$

Here we have also used the fact that $\nabla\tilde{\psi} = \nabla\psi$ (recall that we use ∇ as the sign for the piecewise gradient).

2) Next, recall that

$$\|\nabla\varphi\cdot\mathbf{n}_T\|_{-\frac{1}{2},\partial T}^2 \le C(\|\nabla\varphi\|_T^2 + h_T^2\|\Delta\varphi\|_T^2) = C\|\nabla\varphi\|_T^2,$$
$$\|\tilde{\psi}-\tilde{p}_h\|_{\frac{1}{2},\partial T}^2 \le \|\nabla(\tilde{\psi}-\tilde{p}_h)\|_T^2 + h_T^{-2}\|\tilde{\psi}-\tilde{p}_h\|_T^2$$

for all $T\subset T'\cup T''$, see [24]. Thus the second term of (A.3) can be bounded by

$$\begin{aligned}
&\left\{\sum_{T\subset T'\cup T''}\|\nabla\varphi\cdot\mathbf{n}_T\|_{-\frac{1}{2},\partial T}^2\right\}^{\frac{1}{2}}\left\{\sum_{T\subset T'\cup T''}\|\tilde{\psi}-\tilde{p}_h\|_{\frac{1}{2},\partial T}^2\right\}^{\frac{1}{2}}\\
&\le C\|\nabla\varphi\|_{T'\cup T''}\big(\|\nabla(\tilde{\psi}-\tilde{p}_h)\|_{T'\cup T''}^2 + h_g^{-2}\|\tilde{\psi}-\tilde{p}_h\|_{T'}^2 + h_g^{-2}\|\tilde{\psi}-\tilde{p}_h\|_{T''}^2\big)^{\frac{1}{2}}\\
&\le C\|\nabla\varphi\|_{T'\cup T''}\|\nabla(\tilde{\psi}-\tilde{p}_h)\|_{T'\cup T''},
\end{aligned}$$

where we have employed Cauchy–Schwarz's inequality, the fact that h_T for all $T\subset T'\cup T''$ and h_g are comparable (their ratio is bounded as a function of $\kappa_{\mathcal{T}_h}$ and $C_{\mathcal{G}_h^*}$), and the discrete Poincaré inequality

$$\|\tilde{\psi}-\tilde{p}_h\|_{T^*} \le C h_g\|\nabla(\tilde{\psi}-\tilde{p}_h)\|_{T^*}, \tag{A.5}$$

$T^* = T', T''$, whose use is justified by the fact that Assumption 4.1 (2) holds (thus $\tilde{\psi}-\tilde{p}_h$ is continuous in mean on interior sides of $\mathcal{T}_h|_{T^*}$) and by (A.2a)–(A.2b) (thus $\tilde{\psi}-\tilde{p}_h$ is of zero mean value in T^*), see [29, Theorem 8.1]. Thus the second term of (A.3) is bounded by (A.4) as the first one is.

3) Let $T\in\mathcal{T}_h$ and $e\in\mathcal{E}_T$. Similarly to (2.9), we also have the trace inequality

$$\|\varphi-\varphi_T\|_e \le C h_T^{\frac{1}{2}}\|\nabla\varphi\|_T.$$

Thus, for a given $T\subset T'\cup T''$,

$$\|\tilde{\psi}-\tilde{p}_h\|_{\partial T\cap g}^2 \le C(h_T\|\nabla(\tilde{\psi}-\tilde{p}_h)\|_T^2 + h_T^{-1}\|\tilde{\psi}-\tilde{p}_h\|_T^2).$$

Consequently, the third term of (A.3) is bounded by

$$\begin{aligned}
&\left\{\sum_{T\subset T'\cup T''}\|[\![\tilde{p}_h]\!]\|_{\partial T\cap g}^2\right\}^{\frac{1}{2}}\left\{\sum_{T\subset T'\cup T''}\|\tilde{\psi}-\tilde{p}_h\|_{\partial T\cap g}^2\right\}^{\frac{1}{2}}\\
&\le C\|[\![\tilde{p}_h]\!]\|_g\big(h_g\|\nabla(\tilde{\psi}-\tilde{p}_h)\|_{T'\cup T''}^2 + h_g^{-1}\|\tilde{\psi}-\tilde{p}_h\|_{T'}^2 + h_g^{-1}\|\tilde{\psi}-\tilde{p}_h\|_{T''}^2\big)^{\frac{1}{2}}\\
&\le C\|[\![\tilde{p}_h]\!]\|_g h_g^{\frac{1}{2}}\|\nabla(\tilde{\psi}-\tilde{p}_h)\|_{T'\cup T''} = C\|[\![\tilde{p}_h]\!]\|_g h_g^{\frac{1}{2}}\|\nabla(\psi-\tilde{p}_h)\|_{T'\cup T''},
\end{aligned}$$

where we have employed Cauchy–Schwarz's inequality, the fact that h_T for all $T \subset T' \cup T''$ and h_g are comparable, and the discrete Poincaré inequality (A.5).

4) Let us finally turn to the last term of (A.3). We have, using Cauchy–Schwarz's inequality, the fact that $|[\![\tilde{\psi}]\!]| = |c_{T'} - c_{T''}|$, adding and subtracting $(\tilde{p}_h - \psi)_g$, and employing the triangle inequality,

$$|\langle [\![\tilde{p}_h]\!], [\![\tilde{\psi}]\!] \rangle_g| \leq \|[\![\tilde{p}_h]\!]\|_g \|c_{T'} - c_{T''}\|_g \leq \|[\![\tilde{p}_h]\!]\|_g (\|(\tilde{p}_h - \psi)_{T'} - (\tilde{p}_h - \psi)_g\|_g + \|(\tilde{p}_h - \psi)_{T''} - (\tilde{p}_h - \psi)_g\|_g).$$

Now, using the same technique as in [31, Lemma 7.2] and employing discrete Friedrichs' inequality [29, Theorem 5.4 and Remark 5.9]

$$\|\chi\|_{T^*} \leq C h_g \|\nabla \chi\|_{T^*},$$

$T^* = T', T''$, with $\chi := (\tilde{p}_h - \psi) - (\tilde{p}_h - \psi)_g$, (it is once again crucial that Assumption 4.1 (2) holds), we come to

$$|\langle [\![\tilde{p}_h]\!], [\![\tilde{\psi}]\!] \rangle_g| \leq C \|[\![\tilde{p}_h]\!]\|_g h_g^{\frac{1}{2}} \|\nabla(\psi - \tilde{p}_h)\|_{T' \cup T''}.$$

Combining the above estimates on the individual terms of (A.3), we come to

$$\|[\![\tilde{p}_h]\!]\|_g \leq C h_g^{\frac{1}{2}} \|\nabla(\psi - \tilde{p}_h)\|_{T' \cup T''},$$

whence the assertion of the lemma follows. ∎

REFERENCES

[1] Aarnes, J. E., and Efendiev, Y. An adaptive multiscale method for simulation of fluid flow in heterogeneous porous media. *Multiscale Model. Simul. 5*, 3 (2006), 918–939.

[2] Achdou, Y., Bernardi, C., and Coquel, F. A priori and a posteriori analysis of finite volume discretizations of Darcy's equations. *Numer. Math. 96*, 1 (2003), 17–42.

[3] Ainsworth, M. Robust a posteriori error estimation for nonconforming finite element approximation. *SIAM J. Numer. Anal. 42*, 6 (2005), 2320–2341.

[4] Ainsworth, M., and Rankin, R. Fully computable error bounds for discontinuous Galerkin finite element approximations on meshes with an arbitrary number of levels of hanging nodes. *SIAM J. Numer. Anal. 47*, 6 (2010), 4112–4141.

[5] Arbogast, T., and Chen, Z. On the implementation of mixed methods as nonconforming methods for second-order elliptic problems. *Math. Comp. 64*, 211 (1995), 943–972.

[6] Arbogast, T., Pencheva, G., Wheeler, M. F., and Yotov, I. A multiscale mortar mixed finite element method. *Multiscale Model. Simul. 6*, 1 (2007), 319–346.

[7] Belhachmi, Z. A posteriori error estimates for the 3D stabilized mortar finite element method applied to the Laplace equation. *M2AN Math. Model. Numer. Anal. 37*, 6 (2003), 991–1011.

[8] Bernardi, C., and Hecht, F. Error indicators for the mortar finite element discretization of the Laplace equation. *Math. Comp. 71*, 240 (2002), 1371–1403.

[9] Bernardi, C., Hecht, F., and Mghazli, Z. Mortar finite element discretization for the flow in a nonhomogeneous porous medium. *Comput. Methods Appl. Mech. Engrg. 196*, 8 (2007), 1554–1573.

[10] Bernardi, C., Rebollo, T. C., Hecht, F., and Mghazli, Z. Mortar finite element discretization of a model coupling Darcy and Stokes equations. *M2AN Math. Model. Numer. Anal. 42*, 3 (2008), 375–410.

[11] Brezzi, F., and Fortin, M. *Mixed and hybrid finite element methods*, vol. 15 of *Springer Series in Computational Mathematics*. Springer-Verlag, New York, 1991.

[12] Burman, E., and Ern, A. Continuous interior penalty *hp*-finite element methods for advection and advection-diffusion equations. *Math. Comp. 76*, 259 (2007), 1119–1140.

[13] Carstensen, C., and Hu, J. A unifying theory of a posteriori error control for nonconforming finite element methods. *Numer. Math. 107*, 3 (2007), 473–502.

[14] Creusé, E., and Nicaise, S. A posteriori error estimations of a coupled mixed and standard Galerkin method for second order operators. *J. Comput. Appl. Math. 213*, 1 (2008), 35–55.

[15] Ern, A., Nicaise, S., and Vohralík, M. An accurate **H**(div) flux reconstruction for discontinuous Galerkin approximations of elliptic problems. *C. R. Math. Acad. Sci. Paris 345*, 12 (2007), 709–712.

[16] Ern, A., and Vohralík, M. Flux reconstruction and a posteriori error estimation for discontinuous Galerkin methods on general nonmatching grids. *C. R. Math. Acad. Sci. Paris 347* (2009), 441–444.

[17] Ern, A., and Vohralík, M. A posteriori error estimation based on potential and flux reconstruction for the heat equation. *SIAM J. Numer. Anal.* (2010). DOI 10.1137/090759008.

[18] Ganis, B., and Yotov, I. Implementation of a mortar mixed finite element method using a multiscale flux basis. *Comput. Methods Appl. Mech. Engrg. 198* (2009), 3989–3998.

[19] Girault, V., Sun, S., Wheeler, M. F., and Yotov, I. Coupling discontinuous Galerkin and mixed finite element discretizations using mortar finite elements. *SIAM J. Numer. Anal. 46*, 2 (2008), 949–979.

[20] Glowinski, R., and Wheeler, M. F. Domain decomposition and mixed finite element methods for elliptic problems. In *First International Symposium on Domain Decomposition Methods for Partial Differential Equations (Paris, 1987)*. SIAM, Philadelphia, PA, 1988, pp. 144–172.

[21] Karakashian, O. A., and Pascal, F. A posteriori error estimates for a discontinuous Galerkin approximation of second-order elliptic problems. *SIAM J. Numer. Anal. 41*, 6 (2003), 2374–2399.

[22] Kim, K. Y. A posteriori error estimators for locally conservative methods of nonlinear elliptic problems. *Appl. Numer. Math. 57* (2007), 1065–1080.

[23] Larson, M. G., and Målqvist, A. Adaptive variational multiscale methods based on a posteriori error estimation: energy norm estimates for elliptic problems. *Comput. Methods Appl. Mech. Engrg. 196*, 21-24 (2007), 2313–2324.

[24] Larson, M. G., and Målqvist, A. A posteriori error estimates for mixed finite element approximations of elliptic problems. *Numer. Math. 108*, 3 (2008), 487–500.

[25] Nicaise, S. A posteriori error estimations of some cell-centered finite volume methods. *SIAM J. Numer. Anal. 43*, 4 (2005), 1481–1503.

[26] Ohlberger, M. A posteriori error estimates for the heterogeneous multiscale finite element method for elliptic homogenization problems. *Multiscale Model. Simul. 4*, 1 (2005), 88–114.

[27] Rivière, B., and Wheeler, M. F. A posteriori error estimates for a discontinuous Galerkin method applied to elliptic problems. *Comput. Math. Appl. 46*, 1 (2003), 141–163.

[28] Roberts, J. E., and Thomas, J.-M. Mixed and hybrid methods. In *Handbook of Numerical Analysis, Vol. II*. North-Holland, Amsterdam, 1991, pp. 523–639.

[29] Vohralík, M. On the discrete Poincaré–Friedrichs inequalities for nonconforming approximations of the Sobolev space H^1. *Numer. Funct. Anal. Optim. 26*, 7–8 (2005), 925–952.

[30] Vohralík, M. A posteriori error estimates for lowest-order mixed finite element discretizations of convection-diffusion-reaction equations. *SIAM J. Numer. Anal. 45*, 4 (2007), 1570–1599.

[31] Vohralík, M. Residual flux-based a posteriori error estimates for finite volume and related locally conservative methods. *Numer. Math. 111*, 1 (2008), 121–158.

[32] Vohralík, M. Guaranteed and fully robust a posteriori error estimates for conforming discretizations of diffusion problems with discontinuous coefficients. HAL Preprint 00235810, version 2, submitted for publication, 2009.

[33] Vohralík, M. Unified primal formulation-based a priori and a posteriori error analysis of mixed finite element methods. *Math. Comp.* (2009). Accepted for publication.

[34] Wheeler, M. F., Wildey, T., and Yotov, I. A multiscale preconditioner for stochastic mortar mixed finite elements. Submitted to *Comp. Meth. Appl. Mech. Engrg.*, 2010.

[35] Wheeler, M. F., and Yotov, I. A posteriori error estimates for the mortar mixed finite element method. *SIAM J. Numer. Anal. 43*, 3 (2005), 1021–1042.

[36] Wohlmuth, B. I. A residual based error estimator for mortar finite element discretizations. *Numer. Math. 84*, 1 (1999), 143–171.